Nano Today 35 (2020) 100942

Contents lists available at ScienceDirect

Nano Today

journal homepage: www.elsevier.com/locate/nanotoday

Electro-Hydrodynamic Direct-Writing Technology toward Patterned Ultra-Thin Fibers: Advances, Materials and Applications

Zhenfang Zhang [a,b], Haijun He [c], Wanlin Fu [a], Dongxiao Ji [a,*], Seeram Ramakrishna [a,*]

[a] Faculty of Mechanical Engineering, National University of Singapore, 117574, Singapore
[b] School of Textile Science and Engineering, Xi'an Polytechnic University, 710048, China
[c] Department of Polymer Engineering, Faculty of Mechanical Engineering, Budapest University of Technology and Economics, Műegyetem rkp. 3-9, H-1111, Budapest, Hungary

ARTICLE INFO

Article history:
Received 9 March 2020
Received in revised form 16 June 2020
Accepted 19 July 2020
Available online 8 August 2020

Keywords:
Electro-hydrodynamic direct-writing
Nanofibers
Patterning
Smart materials
Flexible electronics
Biomedicals

ABSTRACT

Fibers, having a large aspect ratio, have become an essential material in human life since the dawn of civilization. Lots of efforts have been made in controlling the fine structure and architecture of fibers for diverse applications. However, great technological challenges remain on patterning fibers with diameters down to tens of nanometers into the desired structure through conventional methods. Electro-hydrodynamic direct-writing (EHDDW) technology shows great potential in depositing the highly aligned micro/nanofibers in a noncontact, direct, and controllable manner which can achieve a real-time adjustment and individually accurate control even on flexible, curved substrates. In this review, beginning with a brief introduction to the history of EHDDW, we first discuss its basic principle and typical apparatus. We continue with a highlight of its rise over the past decades as a powerful technology for the production of nanofibers with versatile compositions and structures. Afterward, we summarize the applications of such "controlled" nanofibers, including their uses as "smart" wearables, energy harvesting/conversion/storage components, and biomedical scaffolds. In the end, we discuss the opportunities and the development directions for this promising area.

Contents

* Corresponding authors at: Faculty of Mechanical Engineering, National University of Singapore, 117574, Singapore
E-mail addresses: jrfive@163.com (Z. Zhang), mpejid@nus.edu.sg (D. Ji), seeram@nus.edu.sg (S. Ramakrishna).

https://doi.org/10.1016/j.nantod.2020.100942
1748-0132/

Introduction

Due to the rapid development of computer science and artificial intelligence (AI) technology, additive manufacturing (AM) is emerging as a revolutionary and commercial manufacturing technology in the past decade [1]. However, the resolution of the conventional AM is restricted to about 50 μm, which limits its further step toward high-precision application scenarios. The material in fiber-shape has great potential in the process of multi-dimension structure because of its high length-diameter ratio. When the diameter decreases down to tens of nanometers, intriguing new characteristics will emerge. The so-called surface effects, size effects, and quantum effects, [2] make these ultra-thin nanofibers attractive and functional for a wide range of applications, including tissue engineering, smart wearables, and flexible electronics [3]. Electrospinning is the most widely used technique to fabricate ultrathin fibers with various precursor materials, from biopolymers to ceramics [4]. However, the patterning of nanofibers by the conventional electrospinning method is still challenging because of the bending instability caused by repulsive electrical force [5]. With the advancement of applications involving nanofibers, further requirements include high alignment degree, precise patterning, and multi-dimension ultrafine structures that are essential for advanced applications. To this end, great efforts have been devoted to developing the electro-hydrodynamic printing (EHDP) technology, built upon the general electrospinning setup.

EHDP integrated conventional electrospinning technique with the layer-by-layer stacking principle of additive manufacturing [6] to be able to print two-dimensional (2D) micropatterns and three-dimensional (3D) microstructures. A typical EHDP system contains a three-axis (XYZ) precise motion system, a high-voltage system, a pneumatic dispensing system, and a thermal control system (Fig. 1a). In the EHDP process, the ink is pumped out through the spinneret to generate a spherical droplet that is deformed into conical shape due to the competition between surface tension and electrical forces. With the increase of charges, a jet will emanate from the apex of the cone [7,8]. Subsequently, the jet will break up into fine droplets or remain intact to form fibers or threads after solution evaporation and melt solidification on the collector [9]. EHDP primarily includes three types (Table 1) of printing modes [8], namely EHD jet (E-jet) printing (dots formation, Fig. 1b), EHD direct-writing (fiber formation, Fig. 1c, d), and electrospray [10] (particle formation, Fig. 1e). The three types of printing modes can be achieved by setting up appropriate parameters, including ink flux, offset height, employed voltage, etc.

EHD direct-writing (EHDDW) belongs to electric field-based printing, which can be dated back to the electrostatic siphon recorder in 1867 (Fig. 2). In the year of 1999, the first direct-write "dip-pen" nanolithography (DPN) [13] was developed to deposit materials of better than 30 nm line width, which is an advantage in fiber deposition over conventional electrospinning. After that, inkjet printing [24] achieved a large area and fast deposition with discrete droplets with micrometer-scale size in 2000, and further improved the production controllability.

At the end of the twentieth century, tremendous efforts start to explore the methods of fiber alignment, including using dynamic collectors [25], auxiliary parallel electrodes [20–21], and magnetized polymeric solution. However, there still exists the limitation in directly, continuously and individually controlling isolated fibers to fabricate high precise patterns and devices. The length of the stable and straight segment of the EHDDW at the initial part of the jet ranges from 500 μm to 3 mm. Therefore, a rather small nozzle-to-collector distance is adopted to obtain high-resolution micro/nanopatterns with directly writing and relatively low voltage, which is the so-called Near-Field Electrospinning (NFES) technique [16]. NFES was reported to succeed in providing the feasibility of controllable electrospinning to realize the direct-writing of straight micro/nanofibers firstly in 2006 [16]. The temporal research focus is largely on increasing the precision of NFES systems and patterning and exploring complex collector substrates [17,22].

Electrohydrodynamic lithography (EHL) is a significant process of EHDDW in 2010. It is a single-step and cost-effective approach for directly patterning of conjugated polymers on solid substrates with high fidelity. Some researchers prepared user-specific micropatterns with parallel lines as well as lattices with a line width of about 2 μm on a flexible substrate [26,27]. For the first time, Rickard et al. fabricated well-defined patterning of conductive polymer structures through combining EHL with tuning the dimensions of architectures, which opened up many opportunities for applications in nano and bio-technology related fields and devices [28].

To overcome the electric breakdown in the NFES system, a mechano-electrospinning (MES) [29] method was presented to deposit fibers in 2012. The fiber diameters were tuned from 400 to 200 nm continuously in a linear relationship by stretching the fibers though the mechanical drawing of a moving substrate while the Taylor cone was kept stable by the lower voltage [19]. Subsequently, the bead-on-string structures were fabricated successfully [30–32]. The investigation of the fabrication mechanism indicates that the force balance between mechanical drawing force and the capillary force leads to the switch of structures. Although MES could fabricate highly aligned nanofiber arrays and complex patterns, it was restricted to the flat area. Additionally, the straight fiber-based structures enable devices to be bendable but not stretchable.

Nonpannal direct-writing offers opportunities for manufacturing multi-dimension curved devices (2014), even on highly curved surfaces (the radius of curvature: ≈ 50–65 μm) [33]. It's feasible to implement 3D movements of the nozzle to maintain a uniform electric field via modifying the EHD printing system [34]. Liu et al. digitally printed large-scale high-resolution photoresist micro/nano-pattern on ultrathin/curved substrates based on metal-network electrodes (MNEs) which are prefabricated via programmable electrohydrodynamic (EHD) lithography [35]. The wavy direct-writing (WDW) method [20] in 2015 and helix-electrohydrodynamic printing (HE-Printing) [36] in 2017 was developed to directly write high-resolution continuously serpentine patterns to meet the requirements for the manufacture of stretchable micro/nanodevices.

The nozzle also plays a critical role in EHDDW through affecting the efficiency, the process parameters, and the fiber morphology. Researchers explored novel nozzles to improve the direct-writing precision, reduce process steps, and increase the efficiency of nanomanufacturing. Laminar sheath gas nozzles [37] were applied to promote the position precision of the direct-written pattern. To improve the printing efficiency and devices with different materials, multi-nozzle printing including parallel nozzles [38], addressable nozzles [39], and revolver nozzles were appeared. Similarly, tip-in-nozzle (conductive or non-conductive), co-axial nozzle, and multi-hole nozzle (always in parallel) printing have also been viable with the vary of nanofiber morphology.

In the meanwhile, multiple voltages and various inks (inorganic inks, organic inks, and composite inks) [36] were also explored to improve printing resolution and efficiency in the EHDDW system. Moreover, other endeavors were also taken to improve the property of the EHDDW system. Suspension Near-Field Electrospinning (SNFES) [22] technique, which implements an automated platform to maneuver the pillar electrodes around the emitter to suspend fibers in the free space between the electrode support structures, was developed to surpass the restriction of the layer-height-limit in 2019. Recently, the uniform field electrospinning (UFES) [23] was proposed as an easy-handling strategy by inserting the electrospin-

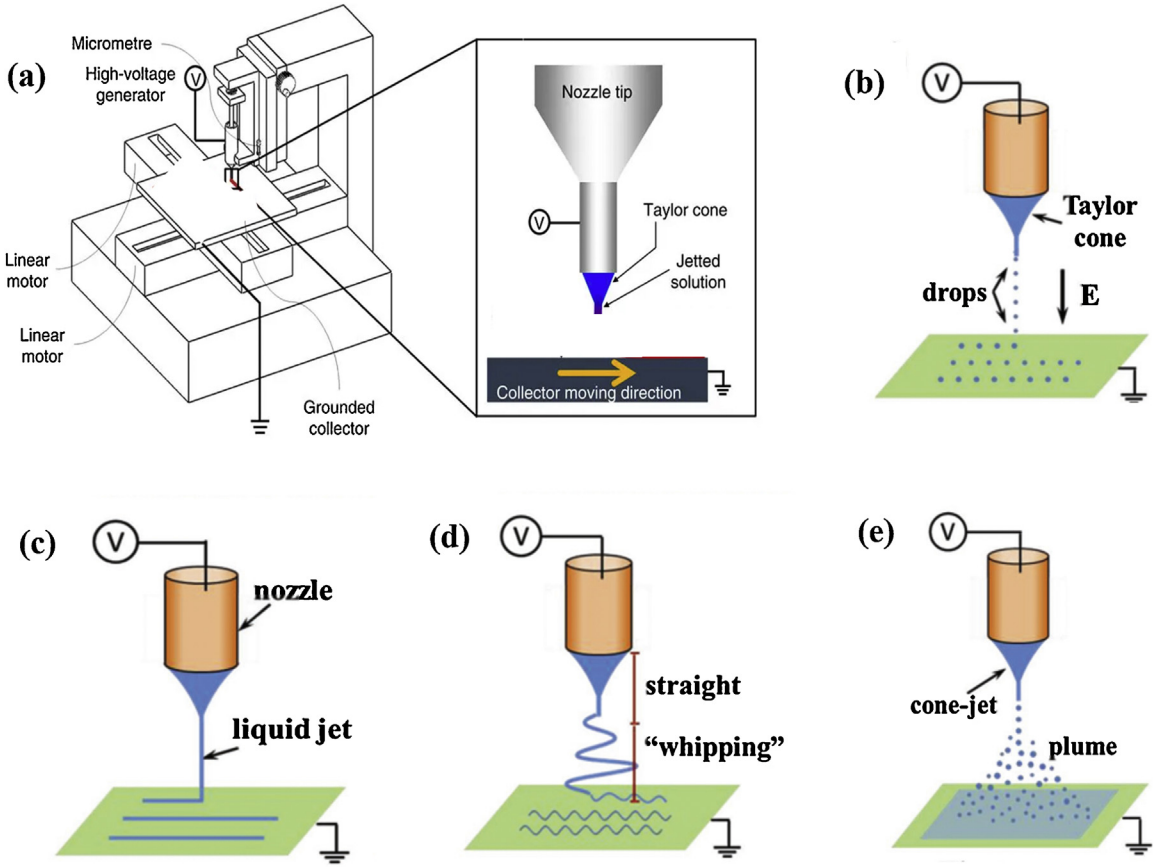

Fig. 1. The apparatus and modes of EHD printing. (a) Schematic diagram of the EHD printing system. Reproduced with permission from [11]. Copyright 2013, Nature. The three types of EHD printing mode are (b) E-jet printing, (c, d) EHD direct-writing and (e) Electrospray. Reproduced with permission from [12]. Copyright 2018, Small.

Table 1
The difference of parameters in voltage, formation, and precision of EHDP

EHD printing mode	Voltage	Formation	Precision
EHD jet printing	DC-Voltage DC-Pulsed Voltage AC-Pulsed Voltage	Droplet (smaller than nozzle)	Sub-micrometer (100 μm-1 nm)
EHD direct-printing	1-3 kV	Fiber	Several micrometers to tens of nanometers
Electrospray	22-34 kV	Particulate material	Nanoscale thickness

ning nozzle into the center of an aided metal plate to create complex geometries.

Therefore, depending on the fabrication characteristics, the devolvement history of EHDDW as shown in Fig. 2 can be classified roughly into original electrospinning (nonwoven fabric), conventional direct writing (part-oriented fiber assembly, including DPN [14] and ink printing [18]), and custom-made direct-writing (high-precision micro/nanostructures, such as scanning tip electrospinning (STES) [37], NFES, and MES). Nowadays, EHDDW has been one of the most popular techniques applied to deposit nanofibers in a large-scale, direct, continuous, and controllable manner.

The attractive capabilities of EHDDW, as well as the related research advances (materials[1,8,61], mechanical properties [3], structure design [6,15,35], producing parameters [12,13,16,39,44,49,58], and applications [41]), have been examined in several reviews before 2014. This review provides a comprehensive overview of the EHDDW technology, including its history, fundamental, innovative modules, and novel applications, especially those developed in the recent five years. We first start with the basic principle of EHDDW technology with emphasis on the modus to achieve the direct writing of nanofibers. Then, we introduce the applied materials and related controlling factors. Additional parts highlight the latest advances of EHDDW applications in fabricating smart materials, electronics, and biomedicals. Last but not least, the review concludes with an overview of key remaining challenges and a summary of opportunities where advances in EHDDW will be critically important for continued progress.

Electro-hydrodynamic direct-writing technology

An EHDDW system includes a voltage supply, an ink supply, a spinning unit, a collector, and a 3D motion system (Fig. 3a, b). Generally, a DC power supply is used to generate an electric field between the collector and the spinning nozzle. The addition of an electric field allows the spinning solution to overcome the surface tension to form a Taylor cone, which in turn forms the nanofiber structure. Different nozzle forms, collector shapes and materials have a significant impact on the spinning process of EHDDW by changing the strength and distribution of the electric field. Therefore, the parameter adjustment of EHDDW is a systematic project. 3D motion system, consisting of a camera and a multi-directional

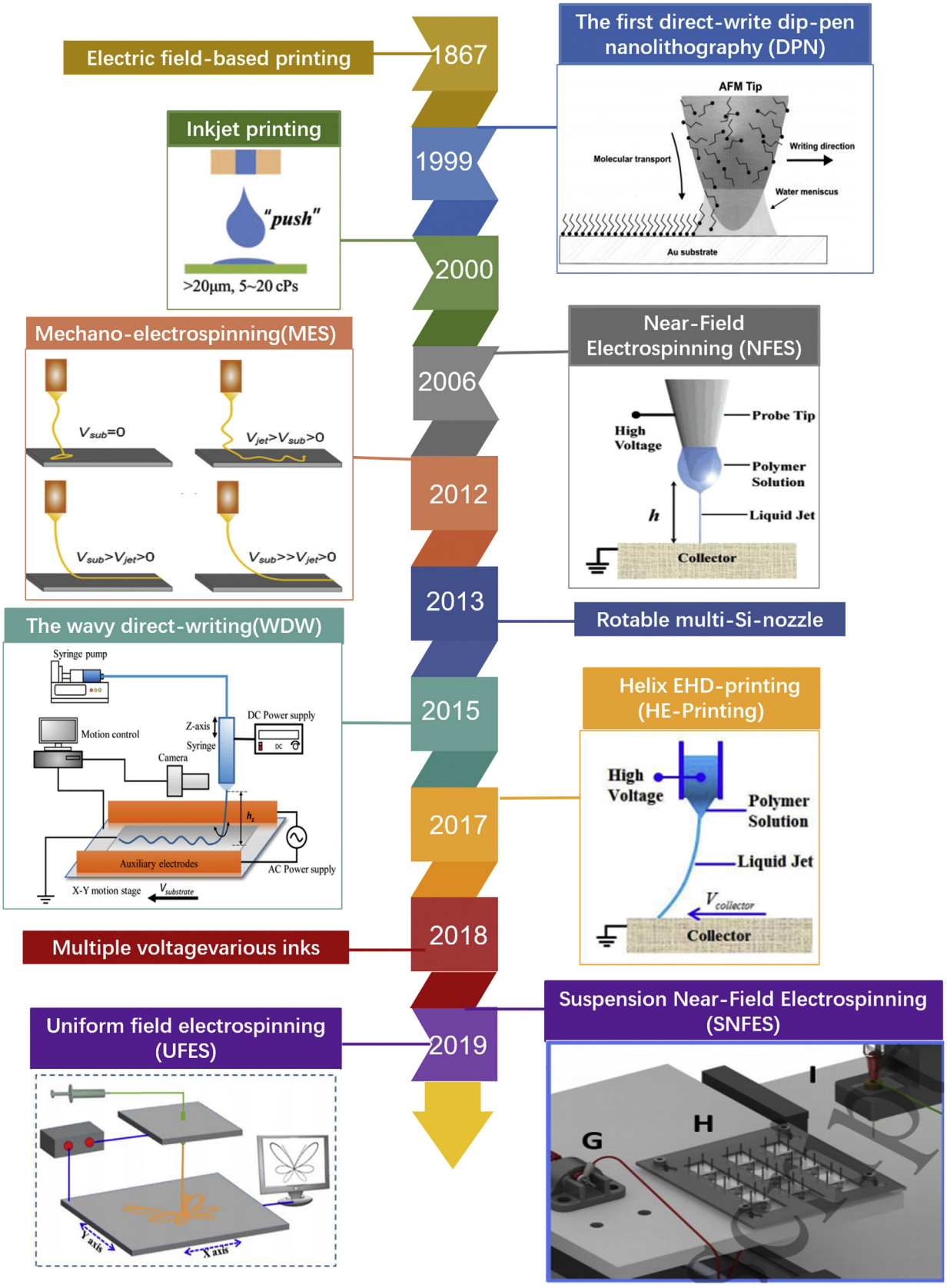

Fig. 2. A brief chronology of the evolution of EHD direct writing.

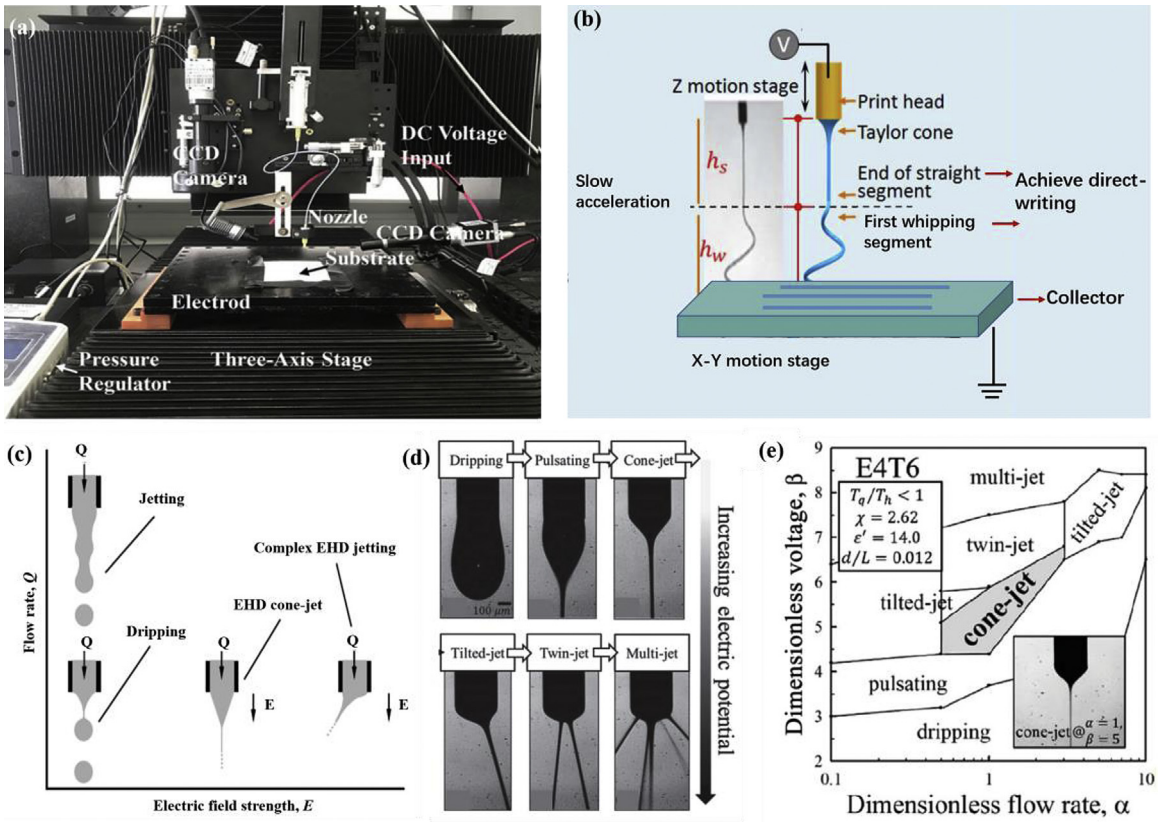

Fig. 3. (a) The experimental setup of the EHDDW method. Reproduced with permission from [46]. Copyright 2019, Journal of Materials. (b) The schematic diagram of a direct-writing process of the EHDDW system. The h_s is the straight segment and h_w is the first whipping segment. Reprinted with permission from [47]. Copyright 2013, Nanoscale. (c) Different modes of jetting, depending on the strength of the electric field and flow rate. Reproduced with permission from [41]. Copyright 2007, Cambridge University Press. (d) The EHD jetting modes with respect to electric potential. Reproduced with permission from [8]. Copyright 2018, Small. (e) Diagram showing the dependence of jetting modes on dimensionless flow parameters. Reproduced with permission from [48]. Copyright 2013, American Chemical Society.

motion system, can achieve accurate deposition of the 2D or 3D spatial structure of the nanofiber through computer modeling.

Patterning mechanism of EHDDW technology

In this part, we will focus on the mechanism of EHDDW, which is mainly including the electrohydrodynamic process (jet formation and its motion behavior) and patterned deposition process. Specifically, during the electro-hydrodynamic process, the ink in the ink supply is first squeezed out of the nozzle dynamically by the pump. With the increase of the electric field, the mobile ions in the ink will be accumulated to regions near the surface of the pendant meniscus, leading to the formation of the conical shape known as Taylor cone [40]. Depending on the difference between the strength of the electric field (E) and the flow rate (Q) (Fig. 3c), liquids can be ejected from a nozzle tip to form different modes of jetting. Initially, the droplet will form "dripping" [41] mode with the help of gravity at low E and Q (Fig. 3d). The "pulsating" jets mode with streams of distinct droplets can be obtained either in conditions $Q<Q_m$ (minimum flow rate in stable cone-jet mode) [42] or when $E<E_c$(critical voltage properties of the ink and the applied back pressure) [43]. Subsequently, the "cone-jet" mode with a continuous stream of liquid will generate when further increase the electric field. Both pulsating jet and cone-jet are able to deposit individual jets, which is crucial toward precise deposition. Further increase of E will lead to the appearance of titled-jet and multiple-jets, which is detrimental to the controlled deposition of the nanofiber. To better choose the process conditions, the jetting maps (Fig. 3e) for different mixtures of solvents were constructed in terms of 6 dimensionless numbers using the Buckingham π theorem. The ejected fluid jet will experience three distinctively different segments in sequence: a rapid stretching and acceleration segment toward the collector, then a slow, short, stable and straight segment near the nozzle, and unstable chaotic whipping segment [44]. In a typical EHDDW system (Fig. 3b), only the stable straight segment and the first whipping segment will be considered to achieve the controlling over the movement of the resulted nanofiber because of the relatively slow acceleration [45]. Therefore, the nozzle-to-collector distance is restricted within the nozzle to the first whipping segment (close to 1 cm) to guarantee the controllable positioning. Meanwhile, reducing the applied voltage to a lower level (generally below 3 kV) allows the solvent to have enough time to evaporate and results in a decrease in diameter.

The patterned deposition process is determined by the coordination of the position of the substrate and the ejection of droplets. However, it is quite complex to achieve high-resolution and controllable deposition of inks, which are greatly affected by every parament in the system (the main aspects including nozzle, pulse, and the direction of the electric field).

Nozzle with smaller inner diameters will improve the precision deposition because sharp nozzle will directly affect droplets size and scaling laws that govern e-jet printing [49]. Sharp nozzle and low E and H (H is the distance between the nozzle and substrate) values should be utilized to reduce lateral deviations induced by the narrow electric-field distributions [50]. Due to the simultaneous influences of applied voltage on droplet size and jetting frequency, pulses of high voltage can enable high-speed printing. Meanwhile, due to the hydrodynamic phenomena inside the capillary, the jetting cannot generate beyond a certain voltage frequency [51]. Thus, it is significant to adjust the applied voltage to make a balance

Table 2
Representative EHDDW technologies for patterning ultra-thin fibers

Phases	Innovation	Approaches	Advances	Limitations
Low precision	Auxiliary electrodes	Rings [54] Lens [55] Two parallel electrodes [56]	Decrease fiber buckling Parallel and align fiber on the air gap	Hardly achieve positioning
	Dynamic collector	Rotating cylinder [57] Disc reel [58] Electrode combined with rotating drum collector [59]	Align individual polymer into parallel arrays Well-aligned nanofibers	Hard to fabricate 2D patterns in a flat area
High planar precision	Scanning tip electrospinning [60]	Silicon tip to dip polymer solution Voltage was 4 – 6 kV Oriented by optical chopper motor	Uniform fiber deposition (With nanofibers 100- 1800 nm)	Limited patterning area Restricted controllability
	Near-field electrospinning [16] (NFES)	Tungsten tip to dip polymer solution Voltage was 600v Tip-to-collector distance was 500μm Movable x-y stage	Direct, continuous, and controllable fiber deposition (with nanofiber 50 – 200 nm)	Restricted-area deposition Limited stretching and thinning of fibers
	Atomic force microscope (AFM)-based voltage-assisted electrospinning [61]	Voltage was 8V spinning distance was 10μm	Assemble single nanofiber	Fiber morphology affected by electric field intensity
	Modified direct-printing (like MES, HE-printing,WDW)	Syringe needle [62] Acupuncture needle tip [63] Manage collector speed [64] Novel nozzles	Deposit diverse orderly patterns Straight and continuous/arc/parallel lines and beads-on-string structures on rigid or flexible substrates Coiled nanofibers Mass production	Hard to achieve controlled continuous patterning on 3D substrates
3D direct writing	Low-voltage near-field electrospinning(LV NFES) [65] EHD 3D-printing [66]	Lower than 600 V Super elastic polymer Steer one-dimensional e-jet actively	Continuously pattern nanofibers 3D substrates Improve the printing accuracy by ten times	Limited materials and resolution Precision decreased when deposited on substrates

between high-speed printing and small droplets. The direct current (DC) voltage in the printing system affects the jetting flowing in one direction but results in varying the dynamics of printing due to the build-up of residual charges on the printed droplets on insulating substrates. Besides, the polarity of the electric field may deviate ejected droplets leading to shifts in the positions of the droplets or satellite droplets. Considering the issues mentioned above, the cumulative buildup of charge on insulating substrates should be avoided because the electric field will be distorted, and droplet trajectories are altered. Methods, such as the utilization of conductive substrate/conductive support and external counterions, can dissipate or eliminate the charges [52]. With the polymer solution consumed gradually [16], the continuous jet in a movable nozzle in the Z-axis stage is drawn at the required speed onto the collector, while the moving stage in programmed x-y direction under computer control is able to fabricate multiple dimensional morphological nanostructures with nanofibers [53].

Representative modus of EHDDW

As aforementioned, the real sense of EHDDW technology is how to control the straight segment and first whipping segment to write micro/nanopatterns precisely, directly, and continuously. Therefore, the appearance of NFES which only utilizes the straight segment to control single fiber in a laboratory is the first modus of EHDDW. During the evolution, a lot of innovations have been devoted to overcoming multiple limitations. The related technologies are listed in Table 2.

NFES is the well-known example to realize EHDDW. In 2006, Sun et al. attained NFES firstly by reducing the nozzle-to-collector distance to 500 μm – 5 cm and applying the voltage bias ranging 600 – 3000 V to construct nanofibers with diameter of 50 – 500 nm (Fig. 4a) [16]. NFES is mainly benefited from the smaller needle-to-collector distance to significantly restrict the bending instability and the 2D motion platform, which not only reduces spinning voltage but also achieves the aim of controllable precision deposition of fibers [67]. According to the investigation in the laboratory, the nozzle-to-collector distance in NFES always ranges 0.5 mm-3 mm [68] (generally below 1 cm), while the self-expelling of electrically charged nanofibers realizes the feasibility of locational control of NFES. In addition, the flow rate of the liquid must be significantly reduced to 0.01 – 1 mL/h to support a stable jet [69].

Despite the development of NFES, it is limited to depositing fibers with predesigned trajectories to form 2D planar fiber structures [65]. To realize 3D microstructures, the nozzle of NFES can be adjusted to move in Z-directions in a layer-by-layer style to overcome the patterning perturbations and bending instabilities under the high electric field strength. In the 3D near-field electrospinning (3DNFES) system, the syringe moves in the Y-Z directions, and the collector moves in the X-direction to form curved fibers when the spinneret changes direction (Fig. 4b) [68]. 3DNFES can achieve relatively large area, continuous and fast deposition of straight fibers with a relatively low applied bias voltage in X, Y, Z directions under the precondition of suitable viscoelastic properties of polymer ink [65,70]. It has tremendous potential in the heterogeneous integration of micro/nanoscale materials to rigid/flexible substrates, especially based on the printed organic nanowire. Overall, NFES can achieve unprecedented controllability at resolutions, compared to the contemporary tools, though it is restricted in the production scale because of the relatively low flow rate, and the obtained fiber diameter is much thicker with less stretching from straight segment.

Different from NFES, Mechano-electrospinning (MES) [29] (Fig. 4c) utilizes an electrical field force that serves to keep the cone stable and mechanical drawing force to decrease diameter and improve the deposition accuracy continuously at a relatively low voltage. The nozzle-to-substrate distance of MES is ranging from 2-

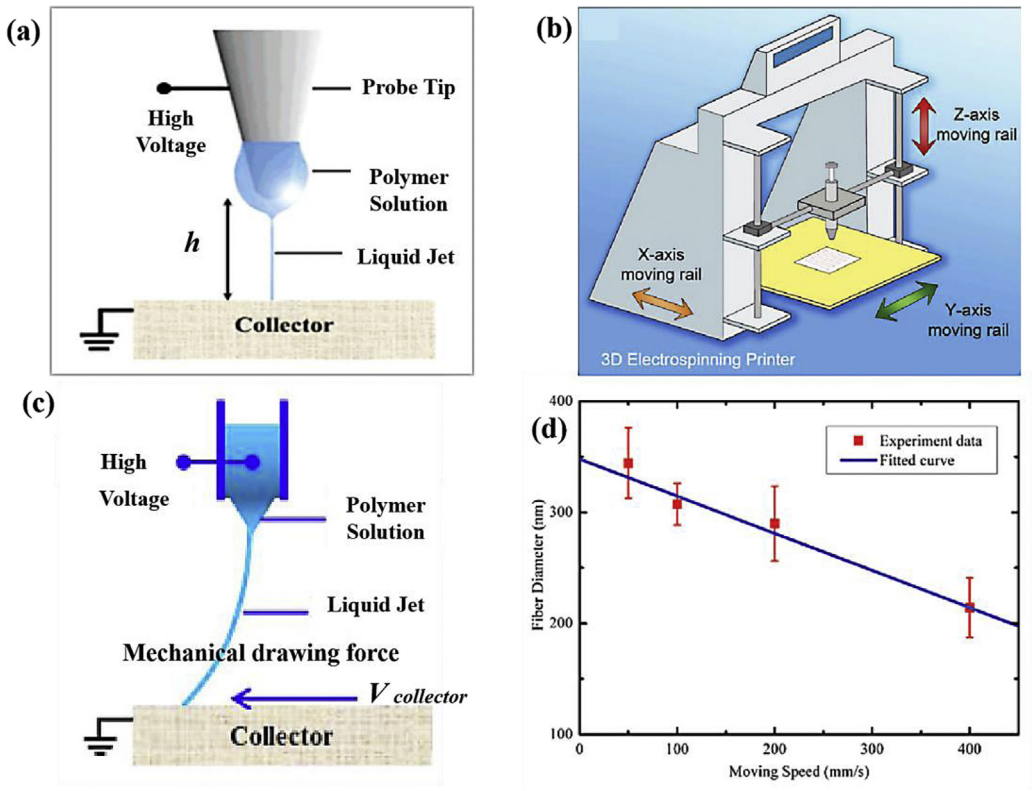

Fig. 4. (a) The typical liquid jet of NFES. Reprinted with permission [47]. Copyright 2013, Nanoscale. (b) Schematic illustration of 3D near-field electrospinning (3DNFES) apparatus created from integrating a 3D printer and NFES. Reproduced with permission from [68]. Copyright 2017, Advanced healthcare materials. (c) The liquid jet undergoes extensive stretching by the moving substrate at a constant speed in MES. Reprinted with permission from [47]. Copyright 2013, Nanoscale. (d) Correlation between fiber diameter and the moving speed of the substrate in MES: The solid line is the result of least-squares fitting to evaluate the diameter trend. The error bar presents the standard deviation of measurement points (color figure available online). Reproduced with permission from [29]. Copyright 2012, Taylor & Francis.

5 mm. Experimentations showed that the fibers, ranging from 200 to 400 nm, will be finer and straighter at a higher drawing force (Fig. 4d). Furthermore, this method can fabricate fibrous nanoarrays (such as straight fiber array and bead-on-string microstructure) [29] continuously with a high local positioning accuracy over a large area on a flat substrate [38].

However, there is always a challenge to obtain a specific serpentine/helical structure with the increasing requirement of stretchable serpentine structure fabrication in many fields, including stretchable energy harvesters [72,73], electronics, and micromechanics [74]. Although several attempts, like assistant manners, and substitute manners [75], have been proposed in different manners to fabricate serpentine micro/nanostructures. Some new uncontrollable problems are generated, and the challenge still exists in manufacturing micro/nano serpentine structures with precise wavelength and amplitude. An innovative direct-writing technique named Helix electrohydrodynamic printing (HE-printing) (Fig. 5a) was thus introduced by Duan et al. [21] They utilized relatively large nozzle-to-collector distance varying from 10 to 50 mm and applied voltage from 1.5 to 3 kV to form nearly circular cross-sectional fiber by accumulating the evaporation and solidification. In the system, certain available methods (such as an electrode ring around the jet or a sharp needle electrode underneath the plate electrode), that can effectively regulate electric field distribution, are adopted to prevent the long and straight segment from being whipping. During the manufacturing process, a long and roughly vertical segment and a helical "coil" are formed (Fig. 5b). Furthermore, the helical fiber can have versatile structures depending on the different collector speeds (Fig. 5c, d). The alternating loops and meandering patterns can be written directly onto the collector by carefully adjusting the system parameters, including applied voltage, nozzle-to-collector distance, and collector speed. This method can realize individually controllable manufacturing of stretchable helical/serpentine micro/nano fibers and has potential in more complex structures like spring-on-spring architecture.

In the EHDDW system, nozzle plays a critical role in fiber morphology. Novel-nozzle system, including parallel nozzles, addressable nozzles [39] and revolver nozzles [81], can not only improve the production efficiency, but it also can fabricate heterogeneous fibers applied in the micro/nano environment. The parallel needle arrays can be made from different materials, such as stainless steel, glass [25] and silicon-based [76] nozzle arrays (Fig. 6a). Han et al. observed the deposition characteristics of double-nozzle and triple-nozzle jets (Fig. 6b) in NFES, from which was concluded that deposition distance was unaffected by the quantity of nozzles [77]. Wang et al. presented dual-nozzle setup which was rotated along the center of the nozzles to fabricate aligned nanofibers in EHDDW (Fig. 6d-f) [79]. Furthermore, a kind of multi-nozzle spinneret was designed by using a printed circuit board (PCB) and drilled holes in solder balls, in which the ball surface accumulated enough electric charges helps to stabilize ejection of jets (Fig. 6c) [78]. Yao et al. designed and fabricated micron aligned Janus fibers comprising non-soluble polycaprolactone (PCL) and soluble polyvinyl pyrrolidone (PVP) using two distinct nozzle systems (Fig. 6g), in which the acriflavine release from PCL fibers spanned over a 4-day period, and release of rhodamine B from PVP fibers was just over 6 hours [80]. The traditional co-axial nozzle system comprises a core needle and another one or two nozzles, which could fabricate nanofibers containing different materials. Liu et al. utilized the coaxial electro-hydrodynamic process to construct a triple-layered, drug-loaded vascular scaffold, of which the wavy structure medial layer prepared with EHDDW can significantly

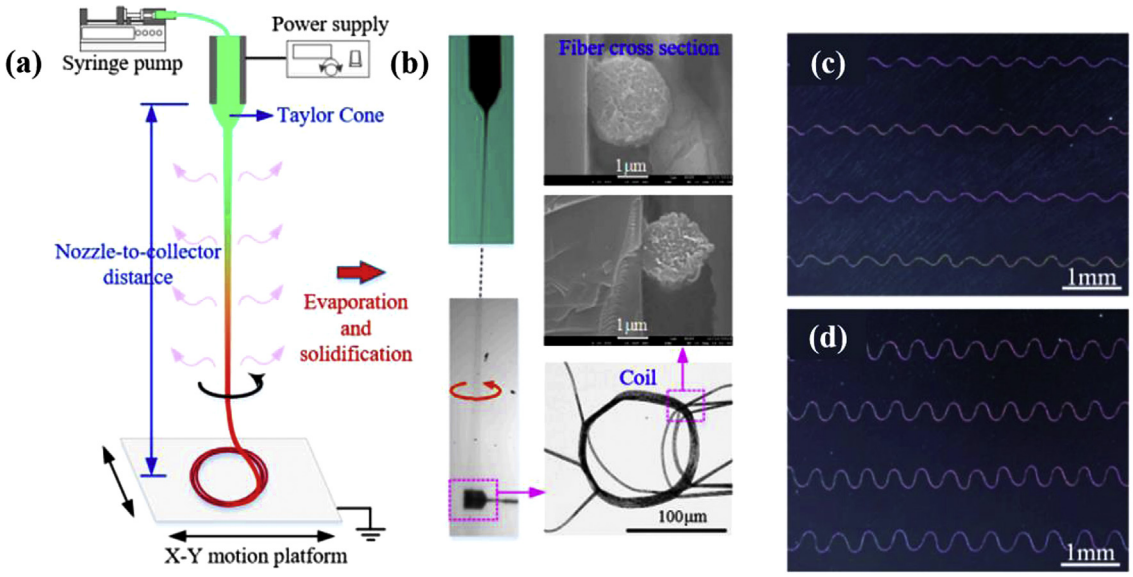

Fig. 5. (a) Schematic diagram of the HE-printing process, and (b) the left column represents the electrospun fiber flying in a helical manner and the right column shows the coil fibers deposited on collector and their cross-sections. (c, d) Highly aligned, large area serpentine micro/nanofibers. Reproduced with permission from [71]. Copyright 2017, Nano Energy.

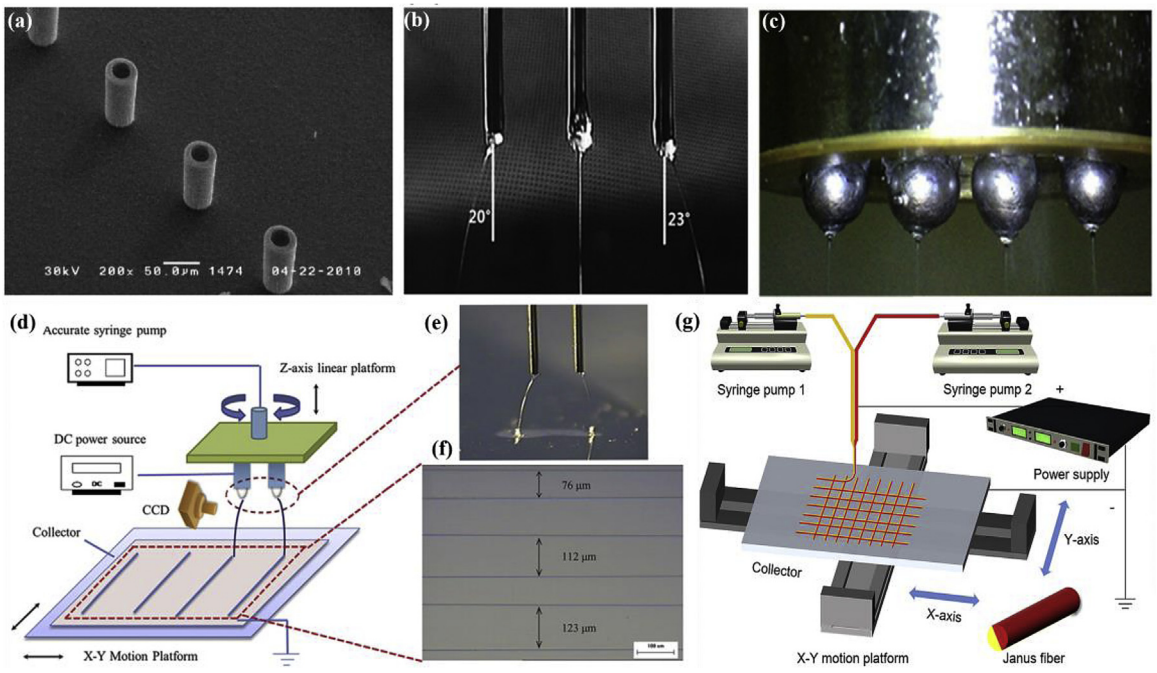

Fig. 6. The novel-nozzle system in EHDDW. (a) Silicon nozzle array. Reproduced with permission from [76]. Copyright 2013, international conference on micro electro mechanical systems. (b) Triple-nozzle jets. Reproduced with permission from [77]. Copyright 2015, AIP Advances. (c) Multi-spinneret structures of 1.5 mm solder ball in NFES. Reproduced with permission from [78]. Copyright 2017, Micromachines. (d) Schematic diagram of dual-nozzle EHDDW system. (e-f) Ejecting behavior of charged jets and direct-written aligned nanofibers with different deposition distances. Reproduced with permission from [79]. Copyright 2017, AIP Advances. (g) Direct writing of Janus fibers. Reproduced with permission from [80]. Copyright 2019, Elsevier.

improve the mechanical properties of the scaffold [82]. Overall, the novel nozzle can fabricate multiple functional composite structures and devices effectively, and it has great potential for industrialization.

Materials for EHDDW

The appropriate material for EHDDW has been demonstrated mainly on organic polymers (solution or melt), small molecules, and composite materials (Table 3). The prepared inks should have a certain viscosity and fluidity. The organic polymer is the most common material used in the EHDDW process, during which the polymer must be dissolved entirely in the appropriate solvent or melted without any degradation [83]. As an appropriate solution, the molecular weight for the polymer should be high enough to generate sufficient chain entanglement, and the polymer should be dissolved by the solvent to evaporate and solidify appropriately [84]. Beyond that, the solution concentration should be suitable. It

Table 3
Polymers used in EHDDW

Polymers	Application	Property	Method (Voltage; Distance)
Poly(vinylpyrrolidone)(PVP)	Insulator layer in multi-layer electronics	Meet the insulation requirement in a fast, and cost-effective method [88]	NFES (1.8kV-2.3 kV; 0.25 mm)
Poly(3,4ethylenedioxythiophene) (PEDOT):poly(styrenesulfonate) (PSS)	Multi-layer Flexible microcircuit	Conductivity improved about 3 times [46]	NFES (2.6kV-3.0 kV; 0.3mm-0.15 mm)
PCL	Tissue engineering	Thinner fibers and pores on the surface [89]	NFES (Printed on hydrogel) (3.5 kV;10 mm)
Poly(lacticacid) (PLA)	Scaffold	Pattern resolution improved to 10 μm [90]	EHD-fused deposition modeling(E-FDM)
Poly(vinylidene fluoride) (PVDF)	Tissue engineering	Sufficient transformation and magnitude [91]	Melt electro writing (MEW) (2.70 ± 0.08 kV; 4.0 ± 0.5 mm)
PP	3D scaffold	Deposit fine (<5 μm) ordered structures [92]	Electrohydrodynamic (EHD) print-patterning
Nylon-6: polytetrafluoroethylene(PTFE)	Fiber-reinforced soft composites (FrSCs)	Elastic modulus improved 40%-260% [93]	NFES
Poly(methyl methacrylate) (PMMA)	Micro/nano integration manufacturing	Stability and deposition precision increased [94]	Melt electrospinning (10 kV-16 kV;6mm-10 mm)
DNA	Bacterial cell	Line width of approximately 160 μm [95]	Electrohydrodynamic direct-patterning
Chitosan	Stem cells	Mechanical properties improved 75% and cell proliferation 25% greater [96]	Coaxial electrohydrodynamic direct-printing
Collagen	Multi-layered scaffold	Mechanical properties improved >3 times [97]	Electrohydrodynamic jet bio-printing (1.7kV – 2.5 kV; core/shore nozzle)
Gelatin	Drug-loaded vascular scaffold	Mechanical properties improved significantly [82]	Coaxial electrospinning and NFES

will not obtain fiber structure when the concentration is too low, while high concentration will cause huge resistance to the jet formation. Besides, the electrical conductivity of the polymer solution should be within a proper range due to the bending instability, during which some ionic compounds can be applied to improve conductivity. In addition, it is advisable to make different polymer phases mixture to improve the operability of the direct-writing process. For example, although some conductive polymers (Such as poly(3,4-ethylenedioxythiophene) and polyaniline) are difficult to be dissolved into solutions due to the rigid backbones, they can be direct-written in solution through mixing with soluble polymers [85–87]. Regarding the prerequisite of the melt polymer, the keys are certain glass transition temperature and thermal degradation temperature. Therefore, the thermoset polymers, proteins, and thermally unstable polymers are not suitable for this situation. To obtain the polymer melt, a heating system is indispensable during the EHDDW process. Due to the polymer melt has lower electrical conductivity and higher viscosity, compared with the polymer solutions, the diameter of the fibers is usually larger. Overall, the melt is not always applied in EHDDW because of its demand for heating system and limitation of fibers diameter, though it is better in precise deposition and safety [69].

Besides the organic materials mentioned above [98,99], the metallic materials and ceramic materials have been a research hotspot recently owing to their potential applications in many important areas such as electronics, photonics, mechanics [100], tissue engineering, and wearables.

The metal inks based on pure metal [2], metal alloy, and metal oxide (such as ZnO, SnO_2 etc.) have been widely utilized to print specific functional micropatterns via EHDDW method (including conductive, electrical, optical properties or chemical reactions, etc.). Han et al. used a few low-melting metal alloys, including Field's metal (32.5% bismuth, 51% indium, 16.5% tin), Wood's metal (50% bismuth, 26.7% lead, 13.3% tin, and 10% cadmium), and solder (48% tin, 32% bismuth, 20% lead) to directly print 2D patterned conductors with sub 50 μm resolution. It showed stable electrical response and self-healing capability (Fig. 7a-c) [101]. In another study, Several types of metal oxide (SnO_2, In_2O_3, WO_3 and NiO) nanofibers (length of a few micrometers) dissolved in alpha-terpineol or ethyleneglycol (15 wt%) solvents were utilized as inks to print highly integrated and multiplexed gas sensor using EHDDW method [102]. Ruggieri et al. prepared parallel arrays of well aligned nitrogen doped TiO_2 nanofibers (3–4 mm long, 300–500 nm diameter) by NFES technology annealed at 400 °C for NO_2 sensing [103]. Similarly, Liang et al. fabricated all metal oxide thin-film electronics(TFTs) (Fig. 7d) based on semiconducting materials (In_2O_3, In-Ga-ZnO(IGZO)), conductive metal oxide (Sn-doped In_2O_3 (ITO)), as well as aluminum oxide (Al_2O_3) gate dielectric at temperature of 350°C by EHDDW, which exhibit excellent electron transport characteristics (average electron mobilities of up to 117 $cm^2\ V^{-1}\ s^{-1}$), negligible hysteresis, excellent uniformity, and stable operation at low-operating voltage [104]. Regarding molten metal, it has extremely higher surface tension and viscosity than other organic materials. Therefore, the required nozzle temperature is generally high to obtain good ink flowability. Nevertheless, EHDDW is still one of the most effective ways to obtain patterned metal nanowires.

Generally, ceramics are not considered to be directly spinnable because they are difficult to form effective fluids [105]. By combining conventional sol – gel processing with EHDDW, the ceramic nanofibers with either a solid, porous, or hollow structure can be obtained (Fig. 7e, f). The typical process to fabricate ceramic nanostructures can be classified into three steps: (i) Preparation for inorganic sol or a solution containing a matrix polymer together with an alkoxide/salt and polymer precursor; (ii) Fabrication of the composite nanofiber consisting of the polymer matrix and salt precursor at room temperature; (iii) Calcination or chemical conversion of the precursor into the desired ceramic at an elevated temperature, with concomitant removal of all organic components from the precursor fibers. There are more than a hundred kinds of ceramics, including CeO_2, SnO_2, SiO_2, VN, $BaTiO_3$, $LiCoO_2$, Co-doped-ZnO, Sb-doped-SnO_2, and a blend of ZnO_2 and SiO_2, etc., have been constructed into fibrous nanomaterials [106].

Control of the EHDDW process

According to the study of the EHDDW system, the process parameters play vital roles in the structures and properties of nanofibers. The key to achieving writing is reducing the bending instabilities and improving the controllability of the single fiber [109]. Several factors affecting the direct-writing process can be

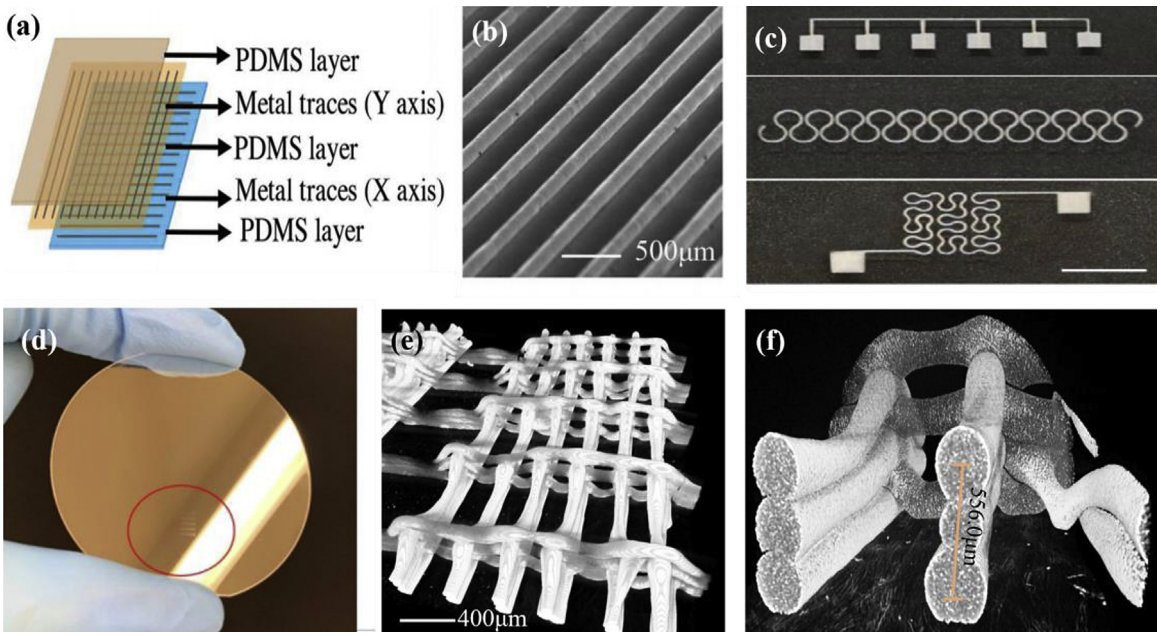

Fig. 7. (a) Schematic of printed projected capacitive touch sensor array. (b) SEM image detailing the printed metallic filaments. Reproduced with permission from [101]. Copyright 2018, Advanced Materials Technologies. (c) Three different high-resolution AgNW patterns. Reproduced with permission from [107]. Copyright 2018, Repository. (d)Direct electrohydrodynamic patterning of high-performance all metal oxide thin-film electronics. Reproduced with permission from [108]. Copyright 2019, ACS. (e) 3D images from a micro-CT scan of a lattice section (f) 3D reconstruction of the high-resolution scan of the lattice of ceramic before calcination. Reproduced with permission from [108]. Copyright 2020, repository.

classified as writing parameters (such as the applied voltage, the collector movement, the spinning distance, flow rate, and needle diameter), solution properties (including, solvent, viscosity, and conductivity) and environmental parameters (e.g. relative humidity and temperature).

Among them, the applied voltage, collector movement, and nozzle-to-collector distance, are the most crucial parameters to be considered to affect the diameters of nanofibers and modify the fabrication accuracy. The relatively low voltage can modify the deposition precision due to its reducing the bending instabilities and the residual charges on the substrate as well as increasing the control of the resulting polymer jet. For example, Bisht *et al.* presented a low voltage NFES with 200 V to continuously write polymeric nanofibers on 2D and 3D substrates [65]. In addition, the electrical drawing force generated by applied voltage also dominates the flow rate of the jetting, namely the thinner nanofiber can be obtained at lower voltage considering the reduced deposition distance in EHDDW system (Fig. 8a).

Due to the enhanced influence of the drawing force on the jetting fiber, the collector movement at relatively high speed also obviously affects the diameters of nanofibers. For example, the average diameter of the resultant fiber significantly decreased from 21.8 $\pm$ 1.2 μm to 17.1 $\pm$ 1.1 μm when the collector speed increased from 50 mm/s to 150 mm/s (Fig. 8b) [80]. Regarding the distance between the needle tip and collector, the relatively greater nozzle-to-collector distance helps to generate smaller fiber diameter and finer fiber patterns (Fig. 8c). However, unstable jet will appear with increasing working distance, which will lead to the mismatching of the jet position [110].

For other controlling factors, the solution concentration will influence the chain entanglement within the polymer, leading to different nanofiber morphology. The particles or polymer beads will generate at low concentration (e.g., 2-15 wt% based on PLGA) due to inability of the weak interactions between the polymer chains. The appropriate concentration of solution based on PLGA for nanofibers generated by EHDDW should be 20-25 wt%, in which the mean diameter of fiber increased from 1.78 $\pm$ 0.4 μm to 3.26 $\pm$ 0.6 μm when the concentration improved from 20 wt% to 25 wt% [111]. As for solution conductivity, the charge transfer from the interior of the solution to its surface may not happen when the conductivity is too low. In one study, with the increase of conductivity of solution from 1.53 to 10.5 mS/cm, the fiber diameter decreased from 214 $\pm$ 19 nm to 159 $\pm$ 21 nm [112]. To reduce the effect of conductivity on the spinning process, the addition of appropriate salt could be a good method. Furthermore, the solvent should be selected carefully. The preferred solvents should dissolve the polymer completely and have a moderate boiling point which is related to the volatility of a solvent. The volatility or vapor pressure of the solvent determines its evaporation rate and thus the solidification rate of the jet. Regarding the solution feed rate, with decreasing the feed speed, it can lead to a decline in the diameter of nanofibers because it will result in lower electric current and a higher surface charge density [113].

Except for the abovementioned factors, several auxiliary methods, such as auxiliary electrodes, auxiliary magnetic fields, novel nozzles, etc., are the innovative controlling methods toward specific patterns and structures. For example, recently, Liashenko et al. achieved ultrafast 3D printing at speed up to 0.5 m s^{-1} in-plane and 0.4 mm s^{-1} in the vertical direction with submicrometer features through locating electrodes around the jet in EHDDW system. The spinning speed was about three to four orders of magnitude faster than techniques providing equivalent feature sizes (Fig. 8c-f) [114].

Environmental conditions, such as temperature and relative humidity, can also influence the fiber structure and morphology. With temperature increases, the solvent evaporation rate increases while the viscosity of the polymer solution decreases to generate thinner nanofibers. It means that the change in temperature will affect average diameter. The relative humidity is another factor to affect electrical charge carried by jet. When the humidity increases, the evaporation of the solvent becomes difficult, thereby reducing the degree of solidification of the fiber. Generally, RH makes the nanofibers thicker or thinner and has a minor effect on the fiber diameter [115]. Zheng et al. used the NFES method to prepare completely uniform PVP fibers. They found that the beaded fibers

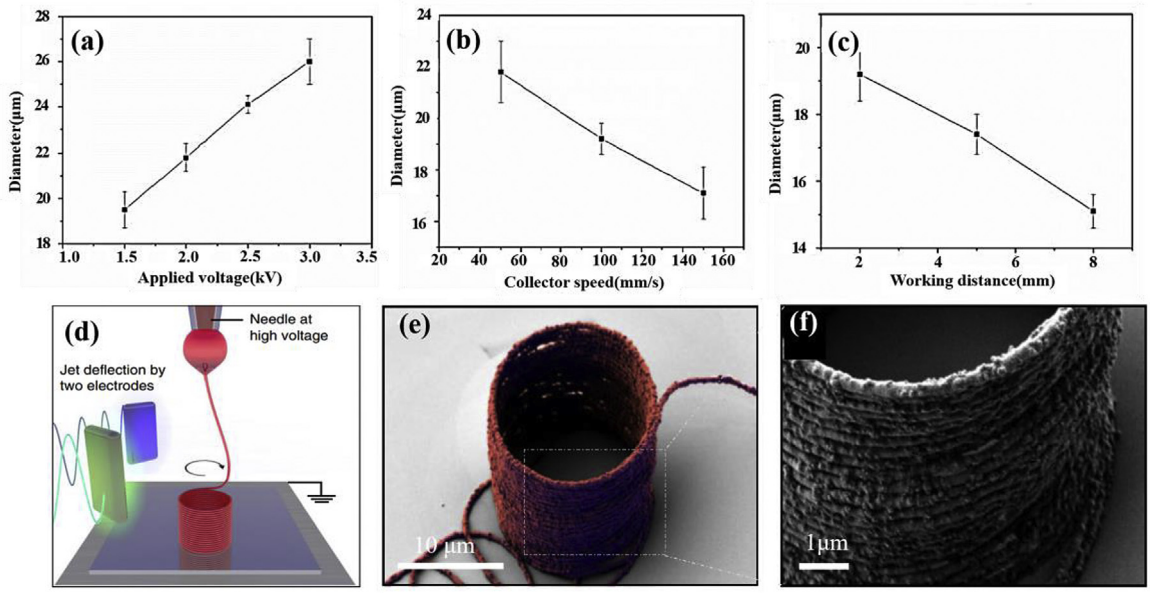

Fig. 8. (a)The mean fiber diameter changed from 19.5 ± 0.8 μm to 26.4 ± 1.0 μm by applied voltage varying in the range of 1.5-3 kV. (b) Effects of collector movement on fiber diameter. (c)The resultant diameters are 19.2 ± 0.8 μm, 17.5 ± 0.5 μm and 15.1 ± 0.5 μm at the working distance of 2, 5 and 8 mm respectively. Reproduced with permission from [80]. Copyright 2019, Journal of Drug Delivery Science and Technology. (d) A schematic of the auxiliary electrodes' 3D direct-printing technology (e, f) SEM micrographs of a PEO-Ag cylindrical structure printed using an ink containing 5 wt% 50 nm Ag nanoparticles. Reproduced with permission from [114]. Copyright 2020, Nature Communications.

mixed with uniform fibers generated when the RH was under 40% [116].

Therefore, the parameter adjustment of EHDDW is a system engineering, and the adjustment method of various factors needs to be comprehensively considered according to the application and the pattern forms. Among them, the addition of auxiliary devices can fundamentally change the distribution of the electric field, which is the main direction of innovation.

Applications

As the EHDDW technique exhibits great superiority in the controllable deposition of a single fiber in precise, continuous, non-contact, high-efficient, and low-cost manner, extensive explorations have been devoted to making breakthroughs for applications in various fields, such as wearables, electronics, biomedicals, etc.

Smart materials

The so-called smart material is a kind of functional material, showing the functions of stimuli-response, shape-memory, self-cleaning, self-healing, sensing, etc. [117] Directly written functional and smart material by EHDDW is particularly attractive for device implementation due to the relatively low assembling cost, easy integration over flexible and large areas [118]. Furthermore, due to the high printing accuracy, the prepared nano-scale materials also exhibit better performance compared with those prepared by the traditional integration methods. Han et al. printed a flexible and stretchable metallic conductor with a sub 50 μm resolution by EHDDW technology. The self-healing capability of the printed conductor (Fig. 9a-d) was demonstrated by heating the broken connection at a temperature of 75 °C for only two minutes with slight pressure [101].

Piezoelectric materials are feasible to convert/supply energy because of the ability to produce electric power and signals when deformed by mechanical force. In 2010, one piezoelectric nanogenerator directly written of poly(vinylidene fluoride) (PVDF) nanofibers via NFES showed better performance in repeatable properties and higher energy conversion efficiency than commercial PVDF thin films [119]. Duan et al. manufactured a kind of nonwrinkled, stretchable piezoelectric generator by directly writing PVDF fibers onto a pre-strained PDMS substrate through MES [73]. It exhibits excellent piezoelectric performance, and the failure strain is 110% higher than that of PDMS (Fig. 9e). This piezoelectric generator may have potential applications in human monitoring and artificial skin by integrating into stretchable electronics. Recently, for the first time, ultrathin ceramic piezoelectric films that are capable of GHz level actuation were created with uniform, continuous traces as narrow as 198 μm and as thin as 128 nm on rigid and flexible substrates via NFES [120]. In another study, electrochromic devices (ECDs) were fabricated by printing a silver grid on indium tin oxide (ITO) film using an EHD method [121]. It was demonstrated that the enhanced conductivity of the silver grid ITO film under low-voltage (1.0 V) operation improved the color quality and response time (Fig. 9f, g), which proved the potential of EHDDW in improving soft ECDs.

Piezoresistive sensors embrace a wide range of applications in soft materials such as smart textiles and artificial skins for the deformation and pressure sensing [122]. Nothnagle et al. fabricated pressure sensor arrays using Poly (3,4-ethylene dioxythiophene):Polystyrene Sulfonate (PEDOT:PSS), a piezoresistive sensing material, by pre-patterning gold or platinum metalized interdigitated comb electrode arrays on a flexible polyimide substrate via electro hydrodynamic printing [123]. It was confirmed that the piezoresistive pressure and strain sensors have sufficient response to strain and linearity on flexible robotic skin due to continuity and good accuracy.

Another significant application in the integration of heterogeneous sensing materials like gas sensors [102] has also been achieved (Fig. 9h, i). In recent times, Zeeshan Yousaf et al. prepared an integrated micro temperature plus humidity sensor using a composite of polyethylene oxide (PEO) and 2D molybdenum disulfide (MoS_2) flakes via EHD printing and electrospray deposition [124]. The sensor achieved a highly sensitive (85 kΩ/%RH) and almost linear response for a wide detection range (0–80% RH)

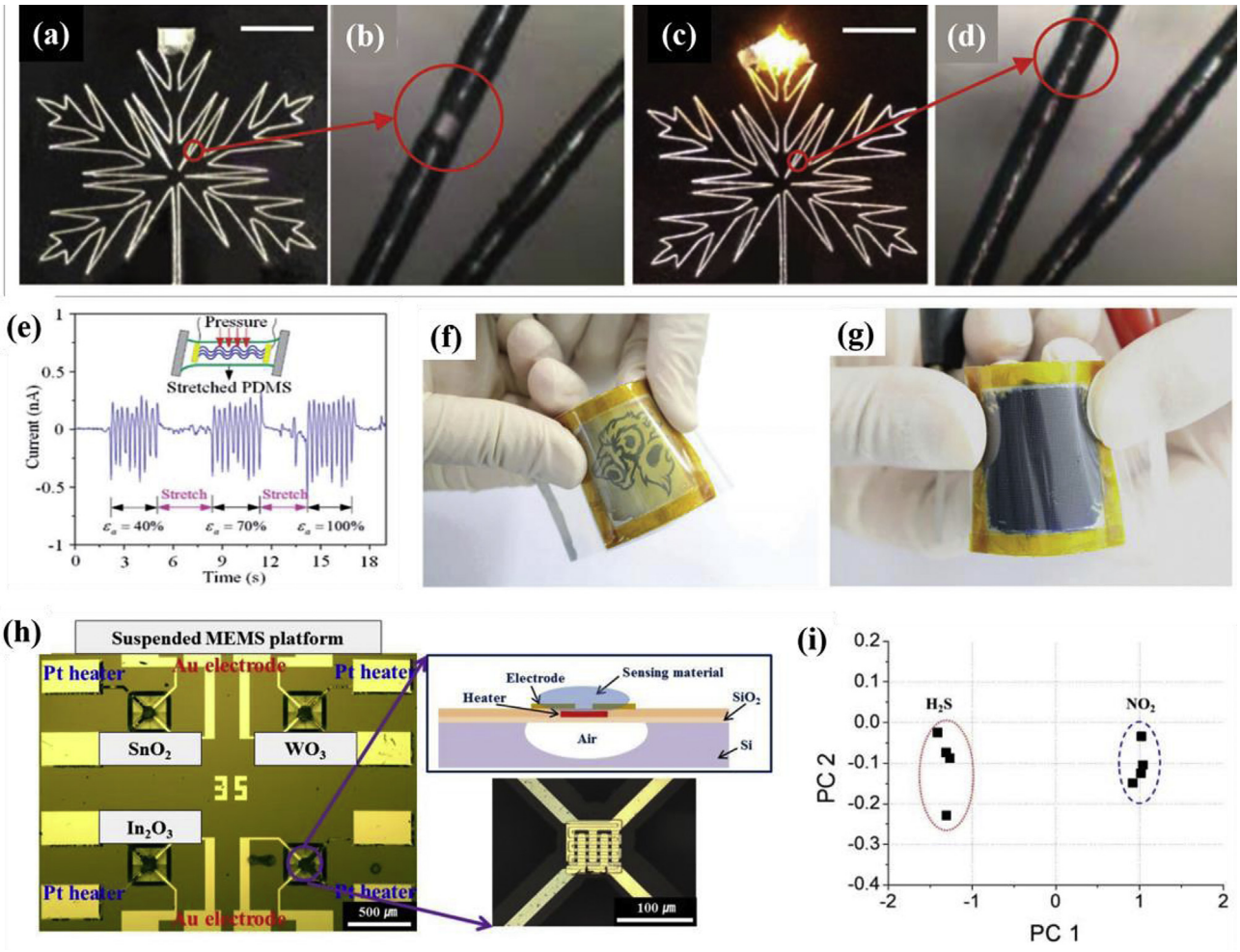

Fig. 9. (a) Self-healing metallic conductor written by EHDDW that connected a battery to a LED. The conductor was intentionally broken by overstretching. (b) Optical photograph of a failure (broken connection) in the conductive path. (c) The circuit recovered from failure after self-healing procedure. (d) Optical image of the healed failure with the broken gap reconnected. Reproduced with permission from [101].Copyright 2018, Advanced Materials Technologies. Scale bar in (a) and (c): 5 mm. (e) Piezoelectric behavior of in-surface buckled fibers on PDMS substrate by EHDDW under constant periodic pressure while with different applied strains. Reproduced with permission from [73]. Copyright 2014, Nanoscale. Images of reversible performance of flexible electrochromic devices by EHD printing from ITO 300 TCE under bent condition (e) bleached state (0 V) and (f) colored stage (1.0 V). Bending radius was 15 mm. Reproduced with permission from [121]. Copyright 2017, Journal of Materials Chemistry C. (h) MEMS gas sensor array fabricated by EHD printing of SnO_2, WO_3 and In_2O_3 nanofibers for low power consumption. The platform size is 3.5 mm x 3.5 mm. (i) PCA results of EHD-printed SnO_2, WO_3 and In_2O_3. Reproduced with permission from [102]. Copyright 2017, Sensors and Actuators B: Chemical.

of relative humidity. For the first time, Lim et al. prepared a novel nano-architecture as gas sensor consisting of 1D metal oxide patterns made of combination Polyvinylpyrrolidone (PVP) and metal nitrates with grid patterns of In_2O_3, Co_3O_4, and NiO nanofibers via NFES, which exhibits an unprecedentedly high gas response (resistance ratio, S_T = 239, T: trimethylamine) and selectivity ($S_T S_E^{-1}$ > 7, E: ethanol) to 5 ppm trimethylamine compared with thin-film counterparts (S_T = 24, $S_T S_E^{-1} \approx 1$) [125]. Wang et al. manufactured micro-scale graphene/polyethylene oxide/sodium dodecyl sulfate composite films through EHDDW for the first time, in which the composite is firstly used in a resistance-based humidity sensor [126]. However, its resistance decreases rapidly as the humidity increases from 63% RH to 100% RH (the response time is less than 2.5 s) due to the porous structure and high specific surface area.

Flexible electronics

Flexible electronics, including light-emitting devices, field-effect transistors and energy harvesting, conversion and storage devices, can serve as ideal platforms for mobile applications because of their unique properties, such as light weight, low cost, high flexibility, and great conformability [127]. A micro pattern is a key component of various flexible functional electronics. Chen et al. fabricated organic micro patterns of poly(3,4-ethylenedioxythiophene):poly(styrenesulfonate)(PEDOT:PSS) mixed material with novel shapes(curve, self-similar, wave structure) using NFES method (Fig. 10a, b). Subsequently, they further directly wrote a flexible multi-layer organic electronic microcircuit pattern of PEDOT:PSS material through repeating positioning through the X and Y axes during direct writing (Fig. 10c), in which the conductivity can be improved effectively about two times with the increase of pattern layers (Fig. 10d) [46]. It demonstrated that the organic micropatterns have flexibility, and maintain continuity of arc contours on the flexible substrate (Fig. 10e) [128]. In another study, the microscale conductive silver features in flexibly tunable resistance were fabricated based on *in situ* reactive Ag-polyethylene oxide (PEO) inks by EHD printing. It successfully achieved features with the smallest size of 27.6 ± 3.4 μm, exhibiting an electrical conductivity of 3.3 × 106 S/min, which demonstrated the printing feasibility of microscale conductive features on various flexible substrates [129].

Harvesting energy from tiny physical motion is increasingly attractive leading to the broad research of energy generators with high flexibility and biocompatibility. Piezoelectric fiber-based

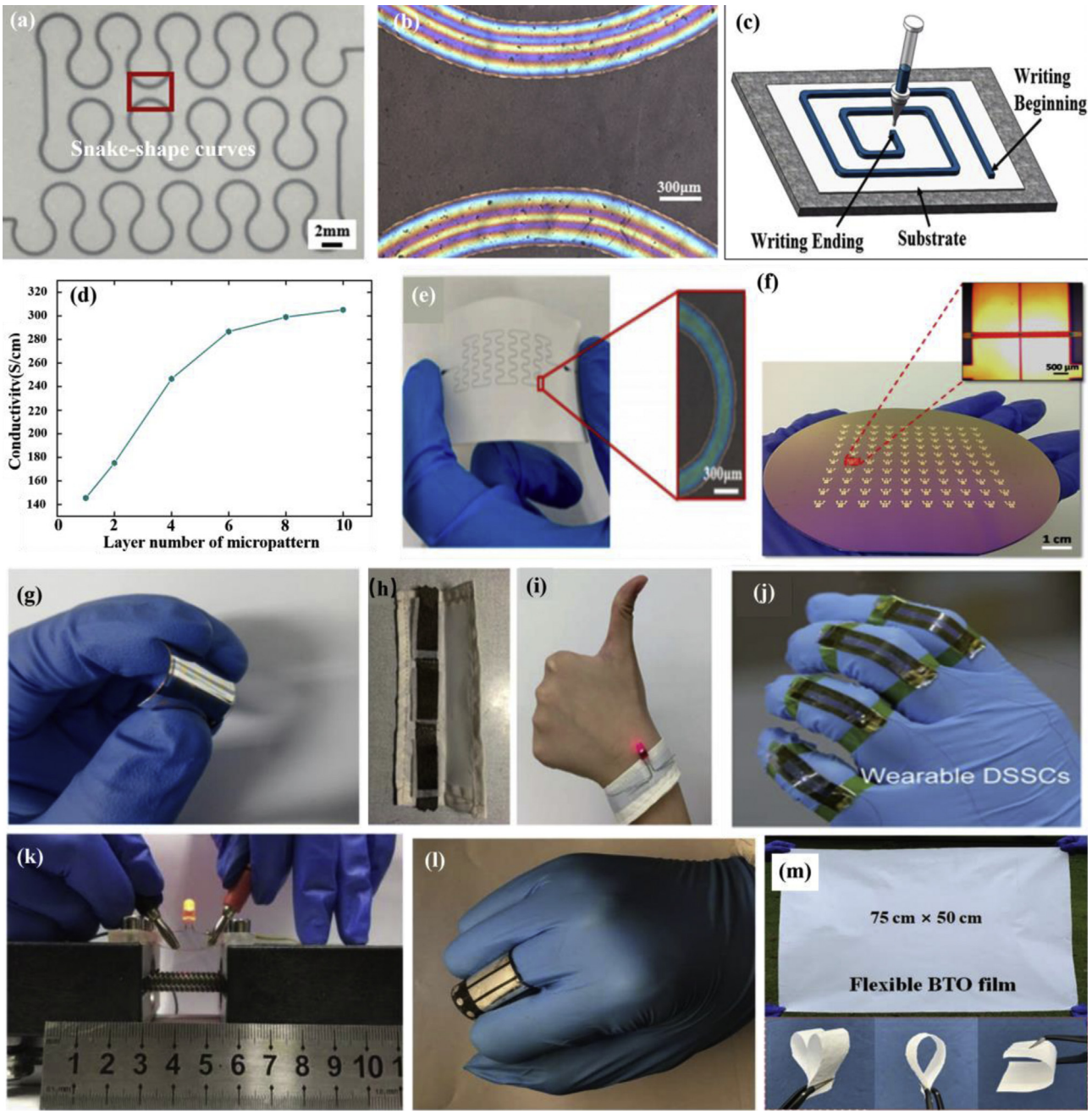

Fig. 10. (a) The snake-shaped microcircuit pattern. (d) The conductivity of the micro-pattern varies with the increase of the number of layers. (b) The partially magnified snake-shaped microcircuit pattern. (c) Repeat positioning through the X and Y axes during direct writing of the multi-layer microcircuit patterns. Reproduced with permission from [46]. Copyright 2019, Journal of Materials Science: Materials in Electronics. (e) Fabricating organic micro patterns of the second-order self-similar structure curve on the flexible insulating substrate. Reproduced with permission [128]. Copyright 2019, Micromachines. (f) Captured digital image of large-area transistor array including 100 EHD-printed P3HT OFETs. The inset image represents an optical microscope image of the P3HT line on Au S/D electrodes and channel. (g) Bending image of flexible EHD-printed P3HT OFETs. Reproduced with permission from [131]. Copyright 2014, ACS Applied Materials & Interfaces. (h) Wearable DSSCs affixed to human fingers. Reprinted with permission from [136]. Copyright 2015, Royal Society of Chemistry. (i) Structural diagram of three pieces of supercapacitor fabrics integrated into a wrist and (j) that powers an LED with 1.6 V turn-on voltage. Reproduced with permission from [135]. Copyright 2016, Royal Society of Chemistry. (k) Demonstration of the stretchable semi-embedded CuNWs TCFs in the light-emitting diode (LED) circuit. (l) Device photograph of the flexible polymer solar cells based on the stretchable CuNWs as electrode and PTB7-th:$PC_{71}BM$ as active layer. Reproduced with permission from [137]. Copyright 2017, ACS Applied Materials and Interfaces. (m) A large-scale BTO film and a demonstration of its flexibility. Reproduced with permission from [138]. Copyright 2019, Advanced Functional Materials.

generators are prepared by combining PVDF fibers and monolayer/bilayer graphene via NFES. The generator exhibited high flexibility and transparency as well as a great performance with an achievable output of voltage/current about 2 V/200 nA [130].

The field-effect transistors (FETs) allow precise electrical control of the charge density, which has great application potential in flexible electronics. In one study, the organic field-effect transistors (OFETs) were fabricated by NFES based on micropatterning poly (3-hexylthiophene) lines without any other polymer binder. The resolution of the printed line and the electrical performance of OFETs were improved through treating a variety of self-assembled monolayers and polymer silk ribbons onto the surface of the substrates (Fig. 10f, g) [131]. Besides, this OFETs showed the commercialization potential with fabricating a large-area transistor

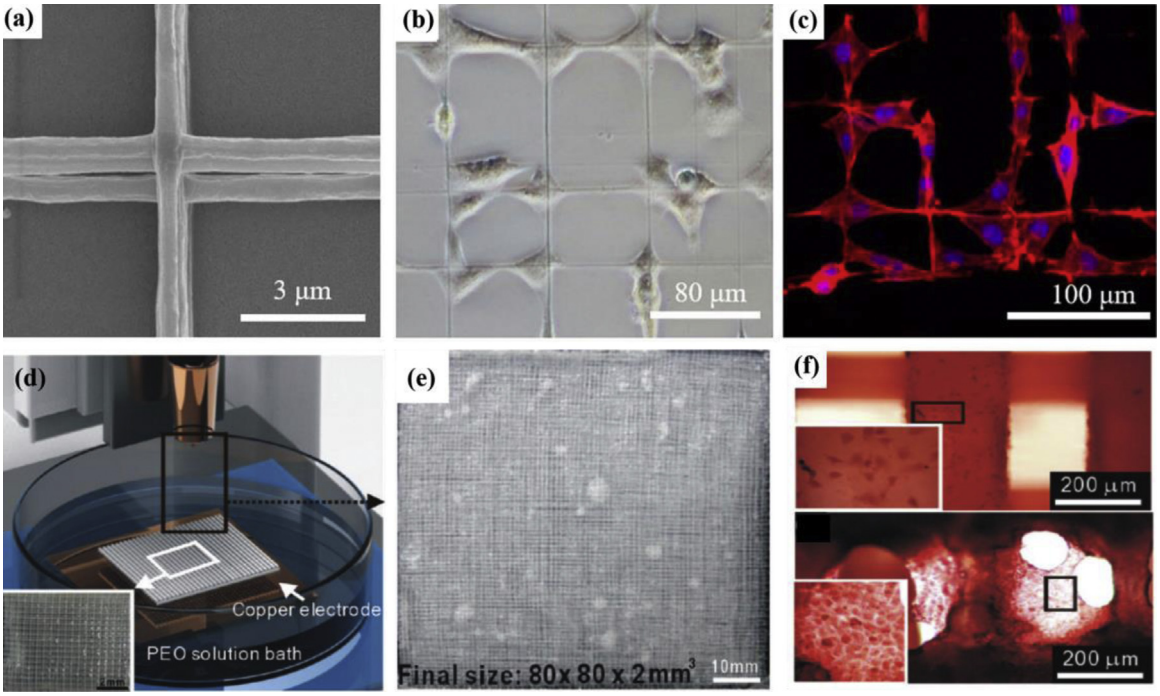

Fig. 11. (a) SEM image of sub-microscale fibrous networks. (b) The cells adhered and grew on sub-microscale fibrous networks, when cultured for 3 days. (c) Fluorescent images of cell-fiber construct stained with phalloidin and DAPI, when cultured for 3 days. Reproduced with permission from [147]. Copyright 2020, Virtual and Physical Prototyping. (d) Fabrication process for a highly roughened 3D PCL scaffold. (e) Optical micrographs of the fabricated scaffold ($80 \times 80 \times 2$ mm^3) (up) and side view of the scaffold (down). (f) Optical micrographs of ARS-staining indicating mineralization for the RP-PCL and EHD-PCL scaffold after 7 days. Reproduced with permission from [146]. Copyright 2011, American Chemical Society.

array, including 100 OFETs, and low-operating-voltage. Furthermore, Li et al. used EHD printing to get a ZnO-based thin-film transistor grounded on indium tin oxide (ITO) transparent conducting electrodes (TCEs) with well-defined patterns (line width ranging from 230 to 30 μm), which has an improvement in its electrical conductivity [132].

A flexible supercapacitor can function as an energy-storage device, which is potential power source for wearable electronics [133]. Shen et al. prepared flexible micro-supercapacitors by directly writing of polypyrrole (PPy) nanofibers on a patterned metal electrode via NFES method. The printed prototype shows a high capacitance of 0.48 m F cm^{-2}, and it is highly flexible with excellent electrochemical performance and cycling stability [134]. Huang et al. obtained a high-performance wearable supercapacitor fabric (Fig. 10i, j) based on flexible metallic fabric (Ni–cotton) with webs of multi-walled carbon nanotubes (MWCNTs) by direct electrospinning [135]. The as-prepared fabric devices showed ultrahigh stability with bending radius of 2 mm, which indicated the remarkable potential applications in wearable electronics for the desired forms.

The electrospun fiber template method gained considerable popularity because it is easy to carry out and exhibits good dimension control in flexible and stretchable micro-systems. Zhou et al. manufactured a highly flexible dye-sensitized solar cell composed of TiO_2 nanotube arrays (TNARs) and a transparent Pt network electrode via templating process [136]. The Pt networks in TNAR based DSSCs exhibit remarkable mechanical flexibility of > 90% photoelectric-conversion efficiency (PCE) after 200 bending cycles, which would be widely used in other wearable, lightweight electronic devices (Fig. 10h). Yang et al. fabricated a large-scale stretchable semi-embedded CuNWs transparent conductive film (TCFs) by electrolessly depositing Cu on the electrospun poly (4-vinylpyridine) (P4VP) polymer template. It showed low sheet resistance (15.6 Ω sq^{-1} at ~82% transmittance), as well as outstanding stretchability and mechanical stability (Fig. 10k, l) [137]. The stretchable semi-embedded CuNWs TCFs maintained effective after stretching with 25% strain and yielded a power conversion efficiency of 4.6% with 0.1 cm^2 effective area, showing great potential for wearable electronic devices. Furthermore, Yan et al. fabricated ultra-flexible crystalline $BaTiO_3$ nanofiber (NF) films via a sol–gel electrospinning method. Polymer NF templates were used to grow perovskite $BaTiO_3$ crystals (Fig. 10m) [138]. The ceramic films have a polymer-like softness of 50 mN, a large Young's modulus of 61 MPa, an elastic strain of 0.9%, and a low density of 28 mg cm^{-3}, demonstrating superior softness without fracture after deformation.

Biomedicals

The EHDDW for biomedical uses, such as tissue repair/regeneration and implant coatings research to combat acute and chronic diseases has aroused increasing interest recently. Kong et al. fabricated 3D fiber-reinforced gelatin methacrylate (GelMA) hydrogel by combining poly (ε-caprolactone)-poly (ethylene glycol) micro fibrous scaffold obtained by NFES with GelMA hydrogel to mimic native cornea for the regeneration of corneal stroma. The influences of differentiation of limbal stromal stem cells (LSSCs) in vitro and in vivo tissue regeneration were studied, which demonstrated that fiber hydrogel and serum-free media synergize for the maintenance of keratocyte phenotype and the regeneration of damaged corneal stroma [139]. Zhang et al. fabricated sub-micron scale biopolymeric patterns with an average fiber size of 193 ± 51 nm to mimic the tiny architectures of native extracellular matrix (ECM) using solution-based EHD printing strategy. It is applicable to biocompatible polycaprolactone (PCL) for the fabrication of water-stable sub-micro scale fibrous architectures [134]. The resultant fibers exhibited unique enhanced cellular performance in adhesion, spreading and orientation compared with fibers made by conventional melt-based EHD printing. Furthermore, it

could be further functionalized by the incorporation of bioactive components for enhanced tissue regeneration.

Along with the importance of highly effective medical therapy for the patients, EHDDW shows great potential to integrate different functional materials to fabricate specific medical materials. Several drugs are difficult to act on the specific part of the body since its poor solubility and bio-applicability. A novel chalcone (KAZ3) with anticancer properties was loaded into mesoporous (SBA-15 and MCM-41) and non-porous (fumed silica, FS) materials via EHD printing and solvent impregnation [140]. The drug dissolution was improved significantly up to 30-fold. The programmed and on-demand approaches were involved to offer a precise control over the release time and the quantity of drug. In another case, a flexible multi-drug membrane consisting of cellulose acetate-ibuprofen (CA-IBU) and cellulose acetate-paracetamol (CA-Para) with an intermediate polycaprolactone (PCL) folding component was fabricated via 3D EHD-printing method. The membrane showed good biocompatibility and extensive application prospects in drug combination therapy and personalized medicine [141]. Wang et al. used EHD printing method to fabricate highly aligned dual-core matrices of graphene-loaded polycaprolactone(PCL)/polyethylene oxide(PEO) materials, exhibiting good biocompatibility and improving PC12 cell migration [142]. Wang et al. fabricated bifunctional micropatterned poly (D,L-lactic acid)/poly (ε-caprolactone) (PDLLA/PCL) membranes uniformly incorporated with Cu_2S nanoflowers for skin tumor therapy and wound healing via patterning co-electrospinning method. The innovative design resulted in high mortality (>90%) of skin tumor cells and effectively inhibited tumor growth in mice, showing great promise for tumor-induced wound healing applications [143].

With the increasing demand for both strength and biocompatibility for an ideal scaffold in tissue engineering, the endothelialization of the vascular scaffold has also become a popular research topic and a cutting-edge study. Gao et al. designed a novel multi-scale scaffold of PCL materials with fiber diameters from 3 μm to 600 μm *via* EHD printing method. The PCL scaffolds with excellent biocompatibility was proved (Fig. 11a-c) [144]. Furthermore, the 3D cell culture was obtained by combining the scaffolds with hydrogel. They found that the patterned fibers enhanced the strength of the scaffolds, and induced the cell migration, which has great potential for tissue engineering. In another study, a double-layer tissue engineering vascular scaffold with a biomimetic structure was fabricated via EHDDW by manually crimping the films with aligned fibers. The paralleled fibers can guide human umbilical vein endothelial cells growth for more than 81% [145]. Furthermore, a 3D biomedical scaffolds (Fig. 11d-f) designed as porous structures for bone tissue engineering was prepared through modified EHDDW technique using poly(ethylene oxide) materials. The biological properties of the scaffold were enhanced 20 times over the cell viability and 6 times over the mineralization. The water-absorption ability was also increased by 400% compared with the scaffold made by rapid-prototype method [146].

Conclusion and outlook

In the past decade, EHDDW has become one of the most promising technology in nanofiber control and the related direct device molding. It has a significant advantage over conventional electrospinning in continuously controlling the morphology, inter- and intra-porosities, dimension, and direction of the nanofiber deposition. Besides, it has wider compatibility with viscous inks to realize high-resolution patterns and high-aspect-ratio 3D micro/nanostructures. Furthermore, its characteristics of non-contact, additive, and reproducible processing lead to high-efficiency and cost-effective solution-processable superiority. This review summarized the latest advances in the methods, materials, and recent investigations of crucial applications of EHDDW technology. The recent remarkable progress of certain applications in wearables, electronics and biomedical products, etc. has been achieved.

Despite the remarkable progress of EHDDW technology in manipulating single fiber has been achieved in the laboratory recently, scale-up fabrication and commercialization still face a number of major challenges that need to be addressed. For example, end effects from neighboring nozzle, disturbance due to surface irregularity of the substrate, and non-conductive material will affect the direct-writing process. In addition, toward the 3D nanodevices preparation, it's still not easy to control the fabrication quality in nano-scale precision. This is also related to the fine structure of the substrate and the adjustment of the electric field. The development direction should be deep into the design and control at nanoscale level.

In the future, great efforts should be devoted on systemically understanding the electric field controlling mechanism, online rheological behavior, and physical property controlling theory, for offering deep insights into the stability, accuracy and one-step fabrication during preparation process. Simultaneously, the integration of experimental and computational works, such as theoretical simulation and path planning technology, is needed to validate and establish the systematical extent of electric filed involved in an EHDDW process. Furthermore, more attention should be paid to the explorations for novel nozzles and their applications, as the form of the nozzle will affect the morphology of fiber and the accuracy of device. To achieve precise and high-speed printing, some methods including multiple nozzles or integration of the EHDDW apparatus may have great potential. Besides, with the increasing demand for multiple application areas, the integration of multifunctional systems to promote the process compatibility with other conventional micro-/nano-fabrication techniques are still noteworthy. The printed electronics remain the most obvious areas of application, like thin-film transistors, in which the functional inks with sufficient conductivity, such as carbon nanotubes, graphene, particle-free silver, and liquid metals, are promising. Biotechnology is another promising area, in which high-resolution 3D direct-printing individual cells and components of an extracellular matrix may have broaden prospect. It is believed that through the unremitting efforts of scientists, EHDDW technology will have broad application prospects in nano-based additive manufacturing.

Declaration of Competing Interest

The authors declare no conflict of interest.

Acknowledgements

This work is supported by NUS Hybrid-Integrated Flexible (Stretchable) Electronic Systems Program Seed Fund (Grant No. R265000628133), Lloyd's Register Foundation, UK (Grant No: R265000553597), and NUS COVID-19 Research Seed Funding (Reference No: NUSCOVID19RG-11). Wanlin Fu thanks the support from the China Scholarship Council (File No. 201806290052).

References

[1] W.E. Frazier, Journal of Materials Engineering and Performance 23 (2014) 1917–1928.
[2] Y. Han, J. Dong, Procedia Manufacturing 10 (2017) 845–850.
[3] E. Tan, C. Lim, Composites Science and Technology 66 (2006) 1102–1111.
[4] G.C. Rutledge, S.V. Fridrikh, Advanced drug delivery reviews 59 (2007) 1384–1391.

[5] D.H. Reneker, A.L. Yarin, H. Fong, S. Koombhongse, Journal of Applied physics 87 (2000) 4531–4547.
[6] B. Zhang, J. He, X. Li, F. Xu, D. Li, Nanoscale 8 (2016) 15376–15388.
[7] J. Choi, Y.-J. Kim, S. Lee, S.U. Son, H.S. Ko, V.D. Nguyen, D. Byun, Applied Physics Letters 93 (2008) 193508–193511.
[8] D. Ye, Y. Ding, Y. Duan, J. Su, Z. Yin, Y.A. Huang, Small 14 (2018) 1703521–1703544.
[9] J. Zeleny, Physical Review 3 (1914) 69–91.
[10] C.J. Hogan Jr, K.M. Yun, D.-R. Chen, I.W. Lenggoro, P. Biswas, K. Okuyama, Colloids and Surfaces A: Physicochemical and Engineering Aspects 311 (2007) 67–76.
[11] S.-Y. Min, T.-S. Kim, B.J. Kim, H. Cho, Y.-Y. Noh, H. Yang, J.H. Cho, T.-W. Lee, Nature communications 4 (2013) 1–9.
[12] D. Ye, Y. Ding, Y. Duan, J. Su, Z. Yin, Y.A. Huang,Small 14 (2018), e1703521.
[13] R.D. Piner, J. Zhu, F. Xu, S. Hong, C.A. Mirkin, science 283 (1999) 661–663.
[14] D. Li, Y. Wang, Y. Xia, Nano letters 3 (2003) 1167–1171.
[15] B. Sundaray, V. Subramanian, T. Natarajan, R.-Z. Xiang, C.-C. Chang, W.-S. Fann, Applied physics letters 84 (2004) 1222–1224.
[16] D. Sun, C. Chang, S. Li, L. Lin, Nano letters 6 (2006) 839–842.
[17] L.S. Carnell, E.J. Siochi, R.A. Wincheski, N.M. Holloway, R.L. Clark, Scripta Materialia 60 (2009) 359–361.
[18] J. Xie, M.R. MacEwan, W.Z. Ray, W. Liu, D.Y. Siewe, Y. Xia, ACS nano 4 (2010) 5027–5036.
[19] N. Bu, Y. Huang, Y. Duan, Z. Yin, Journal of nanoscience and nanotechnology 14 (2014) 3464–3472.
[20] F. Fang, X. Chen, Z. Du, Z. Zhu, X. Chen, H. Wang, P. Wu, Polymers 7 (2015) 1577–1586.
[21] Y. Duan, Y. Ding, Z. Xu, Y. Huang, Z. Yin, Polymers 9 (2017) 434–447.
[22] A.R. Nagle, C.D. Fay, G.G. Wallace, Z. Xie, X. Wang, M.J. Higgins,Nanotechnology 30 (2019), 495301, https://doi.org/495310.491088/491361496528/ab495011b.
[23] Q. Liu, Q. Wu, S. Xie, L. Zhao, Z. Chen, Z. Ding, X. Li, Nanotechnology 30 (2019) 375301–375309.
[24] H. Sirringhaus, T. Kawase, R. Friend, T. Shimoda, M. Inbasekaran, W. Wu, E. Woo, Science 290 (2000) 2123–2126.
[25] Z. Yin, Y. Huang, Y. Duan, H. Zhang, Nozzles for EHD Printing, in: Electrohydrodynamic Direct-Writing for Flexible Electronic Manufacturing, Springer, Singapore, 2018, pp. 117–132.
[26] J. He, F. Xu, Y. Cao, Y. Liu, D. Li, Z. Jin, Applied Physics Letters 105 (2014) 253109–253113.
[27] P. Goldberg-Oppenheimer, U. Steiner, Small 6 (2010) 1248–1254.
[28] J.J.S. Rickard, I. Farrer, P.G. Oppenheimer, Acs Nano 10 (2016) 3865–3870.
[29] N. Bu, Y. Huang, X. Wang, Z. Yin, Materials and Manufacturing Processes 27 (2012) 1318–1323.
[30] N. Bu, Y. Huang, H. Deng, Z. Yin, Journal of Physics D: Applied Physics 45 (2012) 405301–405309.
[31] W. Zuo, M. Zhu, W. Yang, H. Yu, Y. Chen, Y. Zhang, Polymer Engineering & Science 45 (2005) 704–709.
[32] W. Zuo, M. Zhu, W. Yang, H. Yu, Y. Chen, Y.J.P.E. Zhang, Science 45 (2005) 704–709.
[33] W.A. Byeong, K. Kukjoo, K. Mijung, K. So-Yun, H. Seung-Hyun, P. Jang-Ung, Small 11 (2015) 2263–2268.
[34] B. Seong, H. Yoo, V.D. Nguyen, Y. Jang, C. Ryu, D. Byun, Journal of Micromechanics and Microengineering 24 (2014) 097002–097006.
[35] J. Liu, L. Xiao, Z. Rao, B. Dong, Z. Yin, Y. Huang, Advanced Materials Technologies 3 (2018) 1800155–1800163.
[36] Z. Yin, Y. Huang, Y. Duan, H. Zhang, Electrohydrodynamic Direct-Writing for Flexible Electronic Manufacturing, Springer, Singapore, 2018.
[37] J. Zheng, K. Zhang, J. Jiang, G. He, L. Xu, Y. Liu, J. Liu, D. Wu, G. Zheng, AIP Advances 6 (2016) 115304–115311.
[38] Y. Pan, Y. Huang, N. Bu, Z. Yin, Journal of Physics D: Applied Physics 46 (2013) 255301–255308.
[39] J.-S. Lee, S.-Y. Kim, Y.-J. Kim, J. Park, Y. Kim, J. Hwang, Y.-J. Kim, Applied Physics Letters 93 (2008) 243114–243116.
[40] G.I. Taylor, Proceedings of the Royal Society of London, Series A. Mathematical and Physical Sciences 280 (1964) 383–397.
[41] R.T. Collins, M.T. Harris, O.A. Basaran, Journal of Fluid Mechanics 588 (2007) 75–129.
[42] K.-H. Choi, K. Ali, K. Rahman, Chinese Journal of Physics 52 (2014) 799–815.
[43] D.B. Bober, C.-H. Chen, Journal of fluid mechanics 689 (2011) 552–563.
[44] Z.-M. Huang, Y.-Z. Zhang, M. Kotaki, S. Ramakrishna, Composites science and technology 63 (2003) 2223–2253.
[45] D.H. Reneker, A.L. Yarin, Polymer 49 (2008) 2387–2425.
[46] J. Chen, T. Wu, L. Zhang, X. Feng, P. Li, F. Huang, C. Zuo, Z. Mao, Journal of Materials Science: Materials in Electronics 30 (2019) 17863–17871.
[47] Y. Huang, N. Bu, Y. Duan, Y. Pan, H. Liu, Z. Yin, Y. Xiong, Nanoscale 5 (2013) 12007–12017.
[48] A. Lee, H. Jin, H.-W. Dang, K.-H. Choi, K.H. Ahn, Langmuir 29 (2013) 13630–13639.
[49] W.J. Scheideler, C.-H. Chen, Applied Physics Letters 104 (2014) 123315–123318.
[50] J.-U. Park, M. Hardy, S.J. Kang, K. Barton, K. Adair, D. kishore Mukhopadhyay, C.Y. Lee, M.S. Strano, A.G. Alleyne, J.G. Georgiadis, Nature materials 6 (2007) 782–789.
[51] U. Stachewicz, C.U. Yurteri, J.C. Marijnissen, J.F. Dijksman, Applied Physics Letters 95 (2009) 224105–224107.
[52] M.S. Onses, E. Sutanto, P.M. Ferreira, A.G. Alleyne, J.A. Rogers, Small 11 (2015) 4237–4266.
[53] Q. Liu, Q. Wu, S. Xie, L. Zhao, Z. Chen, Z. Ding, X. Li,Nanotechnology 30 (2019), 375301.
[54] X. Cui, L. Li, F. Xu, Applied physics A 103 (2011) 167–172.
[55] Q.P. Pham, U. Sharma, A.G. Mikos, Biomacromolecules 7 (2006) 2796–2805.
[56] W. Teo, S. Ramakrishna, Nanotechnology 16 (2005) 1878–1884.
[57] J.A. Matthews, G.E. Wnek, D.G. Simpson, G.L. Bowlin, Biomacromolecules 3 (2002) 232–238.
[58] A. Theron, E. Zussman, A. Yarin, Nanotechnology 12 (2001) 384–390.
[59] H. Lee, H. Yoon, G. Kim, Applied Physics A 97 (2009) 559–565.
[60] J. Kameoka, R. Orth, Y. Yang, D. Czaplewski, R. Mathers, G.W. Coates, H. Craighead, Nanotechnology 14 (2003) 1124–1129.
[61] Y. Wu, M.S. Johannes, R.L. Clark, Materials Letters 62 (2008) 699–702.
[62] C. Chang, K. Limkrailassiri, L. Lin, Applied Physics Letters 93 (2008) 214–216.
[63] T. Lei, X. Lu, F. Yang, AIP Advances 5 (2015) 041301–041306.
[64] G. Zheng, W. Li, X. Wang, H. Wang, D. Sun, L. Lin, IEEE 5th International Conference on Nano/Micro Engineered and Molecular Systems, IEEE2010 (2010) 284–288.
[65] G.S. Bisht, G. Canton, A. Mirsepassi, L. Kulinsky, S. Oh, D. Dunn-Rankin, M.J. Madou, Nano letters 11 (2011) 1831–1837.
[66] H.D. Bergman, Microsystems Technology, Uppsala University, 2019, pp. 45.
[67] X.-X. He, J. Zheng, G.-F. Yu, M.-H. You, M. Yu, X. Ning, Y.-Z. Long, The Journal of Physical Chemistry C 121 (2017) 8663–8678.
[68] P. Fattahi, J.T. Dover, J.L. Brown, Advanced healthcare materials 6 (2017) 1700456–1700464.
[69] J. Xue, T. Wu, Y. Dai, Y. Xia, Chemical reviews 119 (2019) 5298–5415.
[70] T.D. Brown, P.D. Dalton, D.W. Hutmacher, Advanced Materials 23 (2011) 5651–5657.
[71] Y. Huang, Y. Ding, J. Bian, Y. Su, J. Zhou, Y. Duan, Z. Yin, Nano Energy 40 (2017) 432–439.
[72] Y. Ding, Y. Duan, Y. Huang, Energy Technology 3 (2015) 351–358.
[73] Y. Duan, Y. Huang, Z. Yin, N. Bu, W. Dong, Nanoscale 6 (2014) 3289–3295.
[74] L. Persano, A. Camposeo, D. Pisignano, Progress in polymer science 43 (2015) 48–95.
[75] H.-Y. Kim, M. Lee, K.J. Park, S. Kim, L. Mahadevan, Nano letters 10 (2010) 2138–2140.
[76] K.I. Lee, B. Lim, H. Lee, S.H. Kim, C.S. Lee, J.W. Cho, S.S. Chung, Y.J. Hong, international conference on micro electro mechanical systems (2013) 1165–1168.
[77] W. Han, L. Minhao, C. Xin, Z. Junwei, C. Xindu, Z. Ziming, Aip Advances 5 (2015) 78–88.
[78] C.-T. Pan, K.-C. Tsai, S.-Y. Wang, C.-K. Yen, Y.-L. Lin, Micromachines 8 (2017) 97–112.
[79] Z. Wang, X. Chen, J. Zeng, F. Liang, P. Wu, H. Wang, Aip Advances 7 (2017) 035310–035318.
[80] Z.-C. Yao, J.-C. Wang, B. Wang, Z. Ahmad, J.-S. Li, M.-W. Chang, Journal of Drug Delivery Science and Technology 50 (2019) 372–379.
[81] K. Barton, S. Mishra, K.A. Shorter, A. Alleyne, P. Ferreira, J. Rogers, Mechatronics 20 (2010) 611–616.
[82] Y. Liu, J. Sun, Y. Wang, S. Xie, H. Pu, Y. Peng, L. Xin, Journal of Biomaterials and Tissue Engineering 8 (2018) 665–670.
[83] J. Xue, J. Xie, W. Liu, Y. Xia, Accounts of chemical research 50 (2017) 1976–1987.
[84] C. Luo, E. Stride, M. Edirisinghe, Macromolecules 45 (2012) 4669–4680.
[85] R. González, N.J. Pinto, Synthetic Metals 151 (2005) 275–278.
[86] I.S. Chronakis, S. Grapenson, A. Jakob, Polymer 47 (2006) 1597–1603.
[87] Y.-C. Huang, T.-Y. Lo, C.-H. Chen, K.-H. Wu, C.-M. Lin, W.-T. Whang, Sensors and Actuators B: Chemical 216 (2015) 603–607.
[88] Z. Gao-Feng, P. Yan-Bo, W. Xiang, Z. Jian-Yi, S. Dao-Heng, Chinese Physics B 23 (2014) 066102–066107.
[89] Y. Liu, C. Jiang, Y. Liu, D. Li, Q. Hu, Biosensing and Nanomedicine I.X, International Society for Optics and Photonics (2016) 993010–993019.
[90] B. Zhang, B. Seong, V. Nguyen, D. Byun, Journal of Micromechanics and Microengineering 26 (2016) 025015–025022.
[91] S. Florczak, T. Lorson, T. Zheng, M. Mrlik, D.W. Hutmacher, M.J. Higgins, R. Luxenhofer, P.D. Dalton, Polymer International 68 (2019) 735–745.
[92] M. Rasekh, Z. Ahmad, R. Day, A. Wickam, M. Edirisinghe, Advanced Engineering Materials 13 (2011) B296–B305.
[93] C. Spackman, Rensselaer Polytechnic Institute, American (2016).
[94] Z.J. Yu, L.J. Wang, L.L. Sun, Y.H. Lin, W. Wang, G.F. Zheng, D.H. Sun, Key Engineering Materials, Trans Tech Publ, 2015, pp. 45–51.
[95] J.-H. Kim, D.-Y. Lee, J. Hwang, H.-I. Jung, Microfluidics and nanofluidics 7 (2009) 829–839.
[96] S. Hong, G. Kim, Carbohydrate polymers 83 (2011) 940–946.
[97] M. Kim, G.H. Kim, Chemical Engineering Journal 279 (2015) 317–326.
[98] J.F. Xu, Y.Z. Chen, D. Wu, L.Z. Wu, C.H. Tung, Q.Z. Yang, Angewandte Chemie International Edition 52 (2013) 9738–9742.
[99] W. Nuansing, E. Georgilis, T.V. de Oliveira, G. Charalambidis, A. Eleta, A.G. Coutsolelos, A. Mitraki, A.M. Bittner, Particle & Particle Systems Characterization 31 (2014) 88–93.
[100] Y. Xia, P. Yang, Y. Sun, Y. Wu, B. Mayers, B. Gates, Y. Yin, F. Kim, H. Yan, Advanced materials 15 (2003) 353–389.
[101] Y. Han, J. Dong, Advanced Materials Technologies 3 (2018) 1700268–1700273.

[102] K. Kang, D. Yang, J. Park, S. Kim, I. Cho, H.-H. Yang, M. Cho, S. Mousavi, K.H. Choi, I. Park, Sensors and Actuators B: Chemical 250 (2017) 574–583.
[103] F. Ruggieri, D. Di Camillo, L. Lozzi, S. Santucci, A. De Marcellis, G. Ferri, L. Giancaterini, C. Cantalini, Sensors and Actuators B: Chemical 179 (2013) 107–113.
[104] Y. Liang, THE UNIVERSITY OF MELBOURNE, THE UNIVERSITY OF MELBOURNE, Australia (2019).
[105] T. Subbiah, G.S. Bhat, R.W. Tock, S. Parameswaran, S.S. Ramkumar, Journal of applied polymer science 96 (2005) 557–569.
[106] D. Li, Y. Xia, Nano letters 3 (2003) 555–560.
[107] Y. Han, Industrial and Systems Engineering, North Carolina State University, North Carolina, 2018.
[108] Y. Liang, J. Yong, Y. Yu, A. Nirmalathas, K. Ganesan, R. Evans, B. Nasr, E. Skafidas, ACS nano (2019) 13957–13964.
[109] C. Jiang, K. Wang, X. Jiang, B. Wang, Available at SSRN 3406396, (2019) https://doi.org/10.2139/ssrn.3406396.
[110] G. Kang, G. Zheng, Y. Chen, J. Jiang, H. Chen, X. Wang, W. Li, Y. Huang, J. Zheng, Micromachines 11 (2020) 128–134.
[111] O. Husain, W. Lau, M. Edirisinghe, M. Parhizkar, Materials Science, Engineering: C 65 (2016) 240–250.
[112] C. Zhang, X. Yuan, L. Wu, Y. Han, J. Sheng, European polymer journal 41 (2005) 423–432.
[113] C.-J. Li, Y.-J. Li, J.-N. Wang, J. Cheng, Chemical engineering journal 220 (2013) 294–301.
[114] I. Liashenko, J. Rosell-Llompart, A. Cabot, Nature Communications 11 (2020) 1–9.
[115] S. De Vrieze, T. Van Camp, A. Nelvig, B. Hagström, P. Westbroek, K. De Clerck, Journal of materials science 44 (2009) 1357–1362.
[116] Z. Jie, L. Yun-Ze, S. Bin, Z. Zhi-Hua, S. Feng, Z. Hong-Di, Z. Zhi-Ming, H. Jia-Yin, Chinese Physics B 21 (2012) 048102–048107.
[117] D.J. Leo, Engineering analysis of smart material systems, John Wiley & Sons, 2007.
[118] J. Oliveira, V. Correia, H. Castro, P. Martins, S. Lanceros-Mendez, Additive Manufacturing 21 (2018) 269–283.
[119] C. Chang, V.H. Tran, J. Wang, Y.-K. Fuh, L. Lin, Nano letters 10 (2010) 726–731.
[120] B. García-Farrera, L.F. Velásquez-García, 20th International Conference on Solid-State Sensors, Actuators and Microsystems & Eurosensors XXXIII (TRANSDUCERS & EUROSENSORS XXXIII), IEEE2019 (2019) 1651–1654.
[121] J. Lee, Y. Lee, J. Ahn, J. Kim, S. Yoon, Y.S. Kim, K.Y. Cho, Journal of Materials Chemistry C 5 (2017) 12800–12806.
[122] S.S. Kumar, A.K. Ojha, B. Pant, Microsystem Technologies 22 (2016) 83–91.
[123] C. Nothnagle, J.R. Baptist, J. Sanford, W.H. Lee, D.O. Popa, M.B. Wijesundara, Next-Generation Robotics I.I.; and Machine Intelligence and Bio-inspired Computation: Theory and Applications IX, International Society for Optics and Photonics (2015) 949403–949410.
[124] H.Z. Yousaf, S.W. Kim, G. Hassan, K. Karimov, K.H. Choi, M. Sajid, Sensors and Actuators B: Chemical (2020) 127680–127701.
[125] K. Lim, Y.-M. Jo, J.-W. Yoon, J.-H. Lee, Journal of Materials Chemistry A 7 (2019) 24919–24928.
[126] S. Wang, X. Mei, J. Cao, D. Sun, S. Wang, Journal of Physics D: Applied Physics 52 (2019) 175307–175314.
[127] Y. Yang, W. Gao, Chemical Society Reviews 48 (2019) 1465–1491.
[128] J. Chen, T. Wu, L. Zhang, P. Li, X. Feng, D. Li, Micromachines 10 (2019) 287–300.
[129] Q. Lei, J. He, B. Zhang, J. Chang, D. Li, Journal of Materials Chemistry C 6 (2018) 213–218.
[130] Y.K. Fuh, C.C. Kuo, Z.M. Huang, S.C. Li, E.R. Liu, Small 12 (2016) 1875–1881.
[131] Y.J. Jeong, H. Lee, B.-S. Lee, S. Park, H.T. Yudistira, C.-L. Choong, J.-J. Park, C.E. Park, D. Byun, ACS applied materials & interfaces 6 (2014) 10736–10743.
[132] X. Li, E.M. Jung, K.S. Kim, J.H. Oh, T.K. An, S.W. Lee, S.H. Kim, Electronic Materials Letters 15 (2019) 595–604.
[133] G. Cai, P. Darmawan, M. Cui, J. Wang, J. Chen, S. Magdassi, P.S. Lee, Advanced Energy Materials 6 (2016) 1501882–1501889.
[134] C. Shen, C.-P. Wang, M. Sanghadasa, L. Lin, RSC advances 7 (2017) 11724–11731.
[135] Q. Huang, L. Liu, D. Wang, J. Liu, Z. Huang, Z. Zheng, Journal of materials chemistry A 4 (2016) 6802–6808.
[136] R. Zhou, W. Guo, R. Yu, C. Pan, Journal of Materials Chemistry A 3 (2015) 23028–23034.
[137] X. Yang, X. Hu, Q. Wang, J. Xiong, H. Yang, X. Meng, L. Tan, L. Chen, Y. Chen, ACS applied materials & interfaces 9 (2017) 26468–26475.
[138] J. Yan, Y. Han, S. Xia, X. Wang, Y. Zhang, J. Yu, B. Ding, Advanced Functional Materials 29 (2019) 1907919–1907927.
[139] B. Kong, Y. Chen, R. Liu, X. Liu, C. Liu, Z. Shao, L. Xiong, X. Liu, W. Sun, S. Mi, Nature communications 11 (2020) 1–12.
[140] E. Sayed, C. Karavasili, K. Ruparelia, R. Haj-Ahmad, G. Charalambopoulou, T. Steriotis, D. Giasafaki, P. Cox, N. Singh, L.-P.N. Giassafaki, Journal of Controlled Release 278 (2018) 142–155.
[141] S. Wu, Z. Ahmad, J.-S. Li, M.-W. Chang, Materials Science, Engineering: C 108 (2020) 110393–110401.
[142] B. Wang, X. Chen, Z. Ahmad, J. Huang, M.-W. Chang, Carbon 153 (2019) 285–297.
[143] X. Wang, F. Lv, T. Li, Y. Han, Z. Yi, M. Liu, J. Chang, C. Wu, ACS nano 11 (2017) 11337–11349.
[144] Q. Gao, C. Xie, P. Wang, M. Xie, H. Li, A. Sun, J. Fu, Y. He, Materials Science, Engineering: C 107 (2020) 110269–110280.
[145] Y. Liu, Y. Wang, Y. Zhang, B. Wang, H. Pu, S. Zhong, S. Xie, Y. Peng, J. Luo, T. Yue, Journal of Biomaterials and Tissue Engineering 9 (2019) 298–303.
[146] S.H. Ahn, H.J. Lee, G.H. Kim, Biomacromolecules 12 (2011) 4256–4263.
[147] B. Zhang, J. He, Q. Lei, D. Li, Virtual and Physical Prototyping 15 (2020) 62–74.

Zhenfang Zhang received his Master's degree at Xi'an Polytechnic University. He is currently working with Prof. Seeram Ramakrishna and Dr. Dongxiao Ji at National University of Singapore. His research includes wearables, electrospinning and 3D printing.

Haijun He is currently a Ph.D. student at the Department of Polymer Engineering, Budapest University of Technology and Economics in Hungary. He obtained his B.Sc. and M.Sc. degree in Textile Engineering and Textile Materials at Xi'an Polytechnic University (in China) in 2014 and 2017, respectively. He started his Ph.D. study with the Stipendium Hungaricum Scholarship funded by the Tempus Public Foundation (in Hungary) and China Scholarship Council (in China) in 2017. His research interests are in the development of new electrospinning methods for the scale-up of the nanofiber productivity, polymeric composites reinforced with nanofibers, 3D printing, and smart/functional nanomaterials.

Wanlin Fu obtained her B.Sc. of Chemical Engineering at Southeast University in 2015. She is pursuing her Ph.D. at Southeast University. In the fall of 2019, she joined the Seeram group at National University of Singapore as a visiting Ph.D. student supported by the China Scholarship Council. Her research interests include new synthesis and modification approaches for functional nanomaterials based on electrospinning towards a cleaner environment and sustainability.

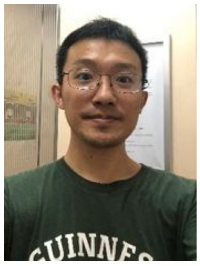

Dongxiao Ji is a research fellow in department of mechanical engineering at National University of Singapore. He received his M.S. and Ph.D. degrees in textile science and engineering from Donghua University in 2012 and 2018, respectively. Dr. Ji is experienced in experimental and analytical research work on heterogeneous catalysis, functional nanofibers, and large-scale electrospinng. His research interests include smart/electronic textiles, functional electrospinning membranes, heterogeneous catalysis, and surface modification for environmental and energy applications.

Seeram Ramakrishna is a professor in department of mechanical engineering at National University of Singapore. He is a Highly Cited Researcher in Materials Science (Clarivate Analytics, 2014; 2015; 2016; 2017; 2018), and in 'Cross-Field' category (2019). A European study placed him among the only 500 researchers in the world with H-index above 150 in the history of science and technology. He is the world's foremost scientist on nanomaterials by electrospinning for uses in diverse fields such as healthcare, energy, water, and environment. His research work over the past three decades led to seminal contributions in novel processing and mechanistic understanding of functional behavior of composite materials, nanofibers, and nanoparticles. He co-authored ~ 1,400 SCI peer reviewed papers which received over 100,000 citations and 150 H-index.